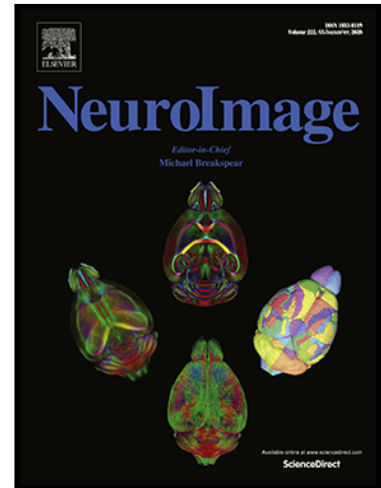# Journal Pre-proof

Signature of Consciousness in Brain-Wide Synchronization Patterns of Monkey and Human fMRI Signals

Gerald Hahn , Gorka Zamora-López , Lynn Uhrig ,
Enzo Tagliazucchi , Helmut Laufs , Dante Mantini ,
Morten Kringelbach , Bechir Jarraya , Gustavo Deco

Please cite this article as: Gerald Hahn , Gorka Zamora-López , Lynn Uhrig , Enzo Tagliazucchi , Helmut Laufs , Dante Mantini , Morten Kringelbach , Bechir Jarraya , Gustavo Deco , Signature of Consciousness in Brain-Wide Synchronization Patterns of Monkey and Human fMRI Signals, *NeuroImage* (2020), doi: https://doi.org/10.1016/j.neuroimage.2020.117470

This is a PDF file of an article that has undergone enhancements after acceptance, such as the addition of a cover page and metadata, and formatting for readability, but it is not yet the definitive version of record. This version will undergo additional copyediting, typesetting and review before it is published in its final form, but we are providing this version to give early visibility of the article. Please note that, during the production process, errors may be discovered which could affect the content, and all legal disclaimers that apply to the journal pertain.

Signature of Consciousness in Brain-Wide Synchronization Patterns of Monkey and Human fMRI Signals

Gerald Hahn[1], Gorka Zamora-López[1], Lynn Uhrig[2,3], Enzo Tagliazucchi[4,5,6,7], Helmut Laufs[5,8], Dante Mantini[9,10], Morten Kringelbach[11,12,13], Bechir Jarraya[2,3,14,15] and Gustavo Deco[1,16,17,18]

[1]Center for Brain and Cognition, Computational Neuroscience Group, Department of Information and Communication Technologies, Universitat Pompeu Fabra, 08018 Barcelona, Spain

[2]Commissariat à l'Énergie Atomique et aux Énergies Alternatives, Direction de la Recherche Fondamentale, NeuroSpin Center, Gif-sur-Yvette, France

[3]Cognitive Neuroimaging Unit, Institut National de la Santé et de la Recherche Médicale U992, Gif-sur-Yvette, France

[4]Institute for Medical Psychology, Christian Albrechts University, 24105 Kiel, Germany

[5]Department of Neurology and Brain Imaging Center, Goethe University, 60528 Frankfurt am Main, Germany

[6]Department of Physics, University of Buenos Aires, Argentina

[7]National Scientific and Technical Research Council (CONICET), Buenos Aires, Argentina

[8]Department of Neurology, Christian Albrechts University, 24104 Kiel

[9]Research Center for Motor Control and Neuroplasticity, KU Leuven, 3001, Leuven, Belgium

[10]Brain Imaging and Neural Dynamics Research Group, IRCSS San Camillo Hospital, Via Alberoni 70, 30126 Venice, Italy

[11]Department of Psychiatry, University of Oxford, Oxford OX3 7JX, United Kingdom

[12]Center for Music in the Brain, Department of Clinical Medicine, Aarhus University, Denmark

[13]Centre for Eudaimonia and Human Flourishing, University of Oxford, UK

[14]University of Versailles Saint-Quentin-en-Yvelines, Université Paris-Saclay, Versailles, France

[15]Neuromodulation Unit, Foch Hospital, 92150 Suresnes, France

[16]Institució Catalana de la Recerca i Estudis Avançats, 08010 Barcelona, Spain

[17]Department of Neuropsychology, Max Planck Institute for Human Cognitive and Brain Sciences, 04103 Leipzig, Germany

[18]School of Psychological Sciences, Turner Institute for Brain and Mental Health, Monash University, Melbourne, Clayton VIC 3800, Australia

Corresponding author:

Gerald Hahn

Center for Brain and Cognition, Computational Neuroscience Group, Department of Information and Communication Technologies, Universitat Pompeu Fabra, C/Roc Boronat 138, 08018 Barcelona, Spain

Telephone number: +34-935-422-629

E-mail: gerald.hahn@upf.edu

During the sleep-wake cycle, the brain undergoes profound dynamical changes, which are manifested subjectively as transitions between conscious experience and unconsciousness. Yet, neurophysiological signatures that can objectively distinguish different consciousness states based are scarce. Here, we show that differences in the level of brain-wide signals can reliably distinguish different stages of sleep and anesthesia from the awake state in human and monkey resting state data. Moreover, a whole-brain computational model can faithfully reproduce changes in global synchronization and other metrics such as the structure-function relationship, integration and segregation across vigilance states. We demonstrate that the awake brain is close to a Hopf bifurcation, which naturally coincides with the emergence of globally correlated fMRI signals. Furthermore, simulating lesions of individual brain areas highlight the importance of connectivity hubs in the posterior brain and subcortical structures in maintaining the model in the awake state, as predicted by graph-theoretical analyses of structural data.

Introduction

Daily life is divided into periods of consciousness with subjective and reportable experience which are repeatedly replaced by periods of consciousness loss (Koch, 2018). These different states of consciousness and their transition are generated and tightly regulated by sophisticated physiological mechanisms residing in the cortex and subcortical structures (e.g. the thalamus, brainstem nuclei and basal forebrain), orchestrating the sleep-wake cycle (Scammell et al., 2017). Pharmacological interventions during anesthesia (Alkire et al., 2008) can interfere with physiology and poise the brain to unconscious dynamics. At the same time, the precise organization of the anatomical connectivity plays a pivotal role in the generation of conscious experience as evidenced in the loss of consciousness after severe brain damage in patients with coma or unresponsive wakefulness syndrome (Gosseries et al., 2014). Understanding how such interplay of the anatomical structure and the physiology of neuronal networks generates different levels of consciousness remains a major challenge in neuroscience research.

To open a window on brain functioning during different levels of consciousness, researchers have traditionally resorted to gain insights from neuronal oscillations that can be captured by recording macroscopic electromagnetic activity either macroscopically (EEG, MEG) (Stevner et al., 2019), mesoscopically (Nir et al., 2011) or by single cell recordings (Steriade et al., 1993). These studies delineate sleep into REM and nonREM sleep which itself is separated into three different stages (N1, N2, N3) each with a distinct electrophysiological profile (Hobson and Pace-Schott, 2002).

More recently, electrophysiological insights have been complemented by fMRI studies which focus on the study of functional relationships between brain areas as measured by correlations between the fMRI signals as a function of time (Mashour and Hudetz, 2018). Such functional connectivity (FC) can be contrasted with the underlying structural connectome (SC) to examine how the variety of pathways constrained by the anatomical connectivity is expressed during different consciousness levels. Overall, the strength of the functional connectivity is largely

reduced during unconscious states, even though specific resting state networks remain intact (Boveroux et al., 2010; Spoormaker et al., 2010). Moreover, during loss of consciousness structural constraints are more rigidly expressed in the functional connectivity as opposed to the awake state (Barttfeld et al., 2015; Tagliazucchi et al., 2016b). In addition, fMRI signals tend to display an organized, wave-like flow across the entire brain with high integration in the awake state, while propagation remains confined to resting state networks with high modularity scores during sleep (Boly et al., 2012; Mitra et al., 2015b; Tagliazucchi et al., 2013). Moreover, it was shown that these correlation metrics are dynamic and show fluctuations across time (Betzel et al., 2016; Fukushima et al., 2018a, 2017; Shine et al., 2016), which are informative about the level of consciousness (Barttfeld et al., 2015; Demertzi et al., n.d.; Haimovici et al., 2017; Uhrig et al., 2018).

Here, we study how large-scale synchronization of the resting state fMRI signal changes across conscious and unconscious states (sleep stages N1, N2, N3 and anesthesia), and whether it can serve as an objective marker for the state of consciousness. Coherence across large parts of the brain has been observed previously in fMRI recordings of humans (Deco et al., 2017b) and monkeys (Liu et al., 2018a; Turchi et al., 2018), and are accompanied by activity changes in neuromodulatory nuclei. We investigate how various degrees of shared large-scale fluctuations relate to metrics such as FC and its relationship with the underlying SC, integration and modularity. The empirical findings are then contrasted with simulations from a whole-brain model and we further examine whether it can reproduce the pattern of global fluctuations seen across different consciousness conditions. Finally, the impact of lesions on global dynamics is studied via in-silico modeling.

Results

In this study, we analyzed brain activity of different vigilance states in two different fMRI datasets, which contain both conscious and unconscious experimental conditions. One dataset was recorded in humans (N = 18) and comprises resting state activity together with different

stages of sleep (N1-N3) with a parcellation of 90 brain areas (Supplementary Table 1). The other dataset stems from monkey recordings (N=3) during wakeful resting and two different levels of propofol anesthesia (moderate and deep) with a spatial resolution of 432 regions (Supplementary Table 2). We searched for a physiological metric that can differentiate conscious from unconscious states and can be explained mechanistically by a whole-brain computational model. Our hypothesis revolved around differences in brain-wide synchronization patterns indicating fluctuations of fMRI activity shared across many brain areas (Scholvinck et al., 2010). To visualize synchronization, we first transformed the fMRI signals into a point process by representing all positive fMRI peaks as discrete events (Tagliazucchi et al., 2012) (Fig. 1A). This approach takes the entire signal across all brain areas into account, irrespective of inter-areal variations of oscillation power in difference frequency band. The raster plots revealed pronounced differences between the awake and unconscious states (Fig 1B). Awake brain dynamics was characterized by frequent large-scale population events that spanned large parts of the brain in both human and monkey resting state data (e.g. Fig. 1B top left, red rectangle). Interspersed were periods with local synchronization and absence of brain wide activity. In contrast, during unconscious states large-scale synchronization was entirely absent with dominant local synchronization between a few areas (e.g. Fig 1B bottom left, blue rectangle) in both human and monkey datasets.

To quantify these varying patterns of global and local synchronization, we applied the Fano factor (FF), a measure widely applied in the analysis of population spiking activity (Brunel and Hakim, 1999; Hahn et al., 2017; Kumar et al., 2008) which captures higher order correlation and global synchrony between discrete events (Fig. 1C, see Methods for a detailed definition). The FF equals ~1, when there is no correlation across brain areas, resembling a random Poisson process (Fig 1C, right). Synchronization across brain regions increases the FF to values >1, with brain wide synchronization events being associated with FF >>1 (Fig 1C, left).

We subsequently computed FFs for sliding windows of different sizes and their distribution for each vigilance state. The distributions decayed exponentially for small window sizes (Fig. 1D),

while larger window sizes revealed that the distribution more generally followed a gamma distribution in human and monkey datasets (Fig. 1E, KS-test; human: window size = 5TR, D = 0.02±0.006, p < 0.001; window size = 25TR, D = 0.03±0.01, p < 0.001; monkey: window size = 5TR, D = 0.06±0.006, p < 0.001; window size = 25TR, D = 0.23±0.07, p < 0.001). The shape parameter (β) of these gamma distributions was subsequently used to quantify the level of synchronization.
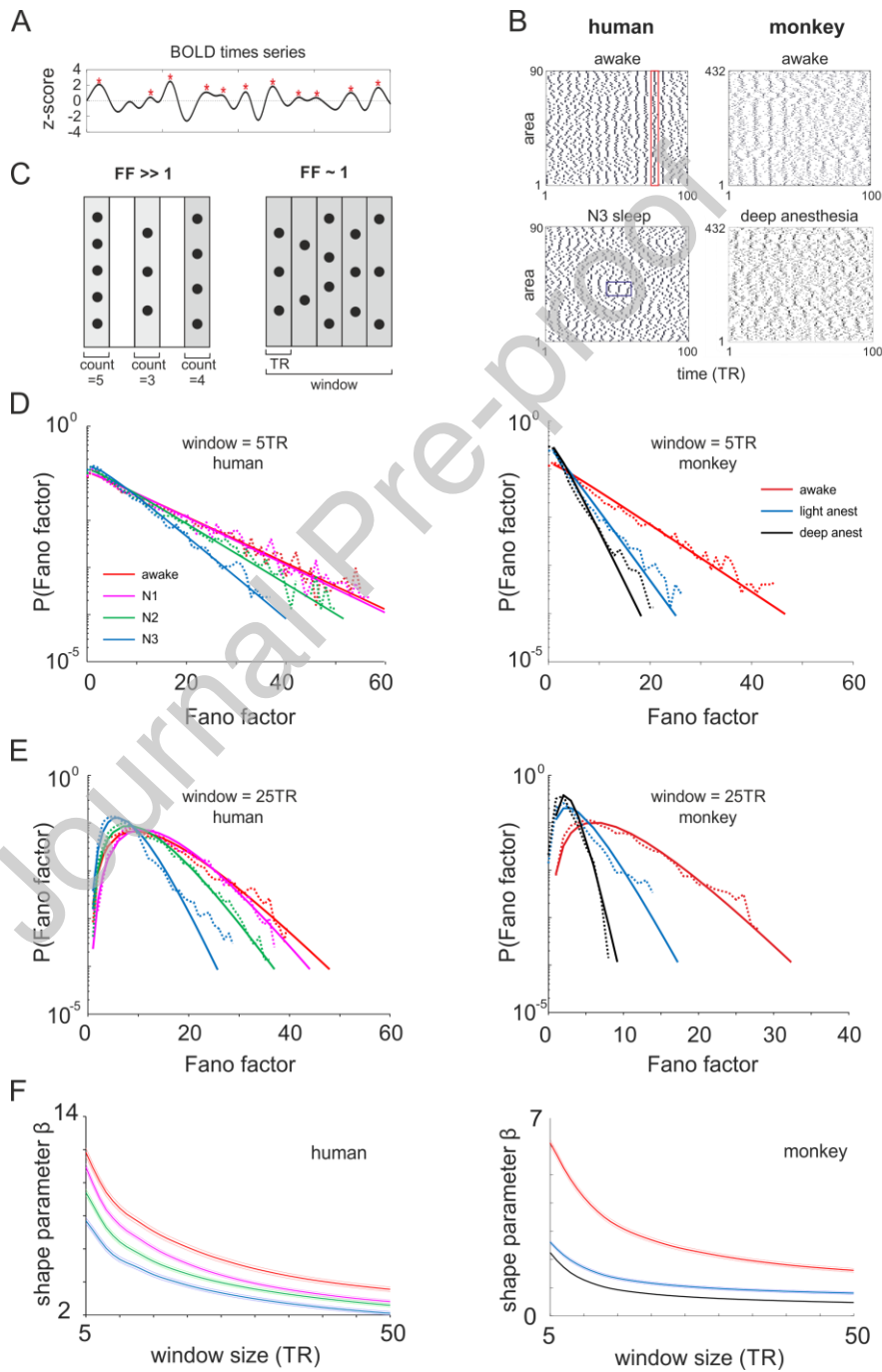
Figure 1: Defining and analyzing global synchronization between BOLD signals. (A) fMRI time series with positive peaks (red asterisks). (B) Examples raster plots of peak time stamps (dots) for a human and monkey dataset, and for two different consciousness levels. Red rectangle: global synchronization event. Blue rectangle: local synchronization event. (C) Raster plots with (left) and without (right) global events for a duration of 5 TR and the corresponding Fano Factor values. (D) Fano factor distributions (dashed lines) of human and monkey recordings and all consciousness levels for a small window size of 5 TR. A fitted gamma distribution (solid lines) is shown for each Fano factor distribution. (E) Same as in D with a larger window size of 25 TR. (F) Mean (±SD) beta values for Fano distributions of all consciousness levels as a function of window size for human and monkey recordings.

Notably, the distributions clearly differed between levels of consciousness in the human and monkey data with the exception of awake and N1 states in humans, which showed a similar synchronization profile (window size = 5TR, one-way rm-ANOVA: F3, 51 = $1.9*10^3$, p < 0.001, ε = 1 in the human and F2,28 = $1.48 * 10^3$, p < 0.0001, ε = 0.6 in the monkey; posthoc test: p < 0.001 for all pairs except for awake vs. N1 with p = 0.99). In the awake state, the distributions were more shallow (Fig. 1D) and right skewed (Fig. 1E) with higher beta values due to a higher prevalence of large-scale synchronization between brain areas. Unconscious states were associated with steeper and more narrow distributions due to missing large-scale synchronization (Figs.1D, E), and reduced beta values. Importantly, the beta parameter also distinguished between different levels of unconsciousness as they progressively decreased, when subjects drifted into deeper levels of sleep or anesthesia. The same results held, when negative fMRI peaks were used for the calculation of FF distributions (Supplementary Fig. 2). To test the robustness of this novel marker, we calculated beta for different window sizes and indeed found that the separation of consciousness states remained unchanged up to a window size = 50 TR (Fig. 1F). Additionally, these findings suggest that the varying levels of large-scale synchronization, as indexed by the FF distribution, could serve as a robust marker for different vigilance states and the depth of unconsciousness.

Computational model

What might be the origin of these declining levels of large-scale synchronization as brain dynamics traverses from awake to gradually deeper levels of unconsciousness? To tackle this

question, we devised a whole-brain computational model that aimed at reproducing these changes in global dynamics. This model simulated local fMRI signals for each brain area of two different parcellations (human: N = 90 areas (Tzourio-Mazoyer et al., 2002), monkey (Paxinos et al., 2009): N=432 areas) using the normalized Hopf bifurcation model (see Methods). The brain areas were connected on the basis of diffusion-tensor imaging data of humans and monkeys (Adluru et al., 2012; Zakszewski et al., 2014). The core parameter of the model is the bifurcation parameter (alpha), which captures the excitability of each node, i.e its responsiveness to incoming input from other brain areas (Supplementary Fig. 3A). We uniformly varied alpha across all brain areas mimicking changes in global excitability mediated by diffusely projecting neuromodulator systems (e.g. acetylcholine, noradrenaline), whose activity is known to change across the sleep-wake cycle (Scammell et al., 2017). Depending on the values of alpha, the model displayed three qualitatively different activity states. When alpha was kept small, the dynamics of the model was governed by synchronization between a few brain areas, but remained free of large-scale synchronization (Fig. 2A, left). This dynamical regime was strikingly similar to the empirical pattern of unconscious states in the monkey and human data (Fig. 1A, bottom). At intermediate values, the dynamics were characterized by periods of asynchronous activity as seen with smaller alpha (Fig. 2A, center), but sporadically interrupted by events of global synchrony. This activity mode was reminiscent of the dynamics seen in the awake humans and monkeys (Fig. 1B, top). Further increase of alpha was accompanied by a dynamical state with highly synchronized and oscillatory activity across the entire model brain (Fig. 2A, right). More generally, the behavior of the model characterizes a bifurcation from local synchrony only (alpha < bifurcation) to global synchronization (alpha > bifurcation) with elements of both types of synchronization close to the bifurcation point (alpha ~ bifurcation).
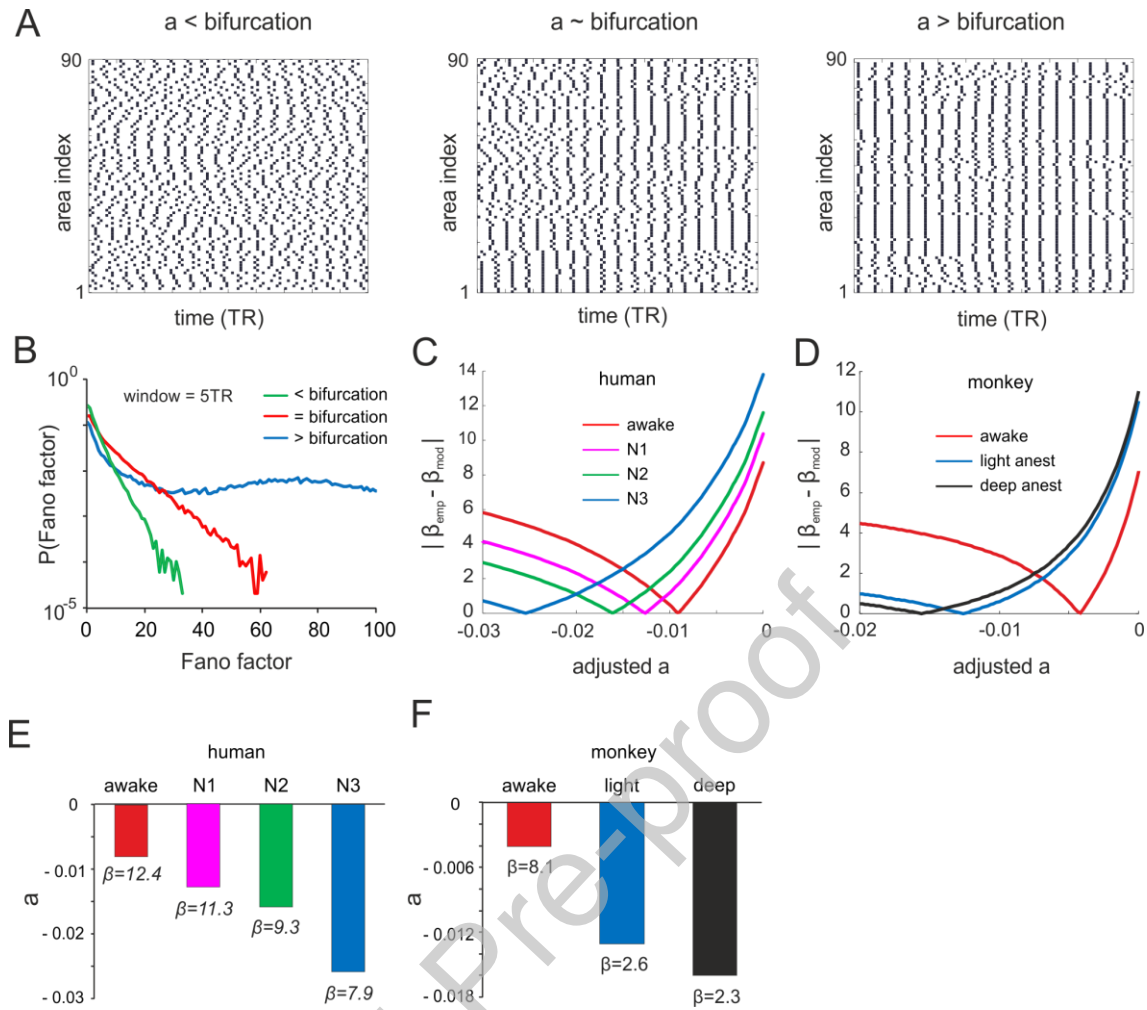
Figure 2. Whole brain model of different consciousness levels. (A) Example raster plots of positive peaks obtained from model simulations of human data with a window size of 5 TR. The results are depicted for three different instance of the bifurcation parameter (a), placing the model below, close or above the bifurcation point. (B) Fano factor distributions for the three different bifurcation parameters shown in (A). Note the pronounced peak in the distribution caused by the global oscillation, when the model is set above the bifurcation point. (C) Fitting of the model to match the Fano factor observed from the empirical human data, expressed as the difference of empirical and model beta values, for different bifurcation parameters and consciousness levels. (D) Same as in (C) for monkey data. (E) Value of the adapted bifurcation parameter (a) as a function of consciousness state in humans. The empirical beta-values of the FF distributions are indicated for each state. (F) Same as in (E) for the monkey data.

Next, we computed the Fano factor distributions for the simulated fMRI signals. These distributions were also governed by gamma distributions which approached an exponential function with small time windows, similar to the empirical counterpart, for alpha < or ~ bifurcation (Fig. 2B). The highly synchronized regime, however, deviated from this behavior

and showed a clear peak in the FF-distribution caused by the global oscillation. After normalization, such that the bifurcation appeared at alpha = 0 (see Methods, Supplementary Fig. 3B), we fitted gamma functions for alpha values < 0 and showed that the obtained beta values increased monotonically as alpha approached the bifurcation point (Supplementary Fig. 3C). Thus, different levels of synchronization in the model mapped directly onto the FF distribution. This allowed us to find the alpha values of the model, where the beta values of empirical and simulated FF distribution were identical, i.e. their difference was close to zero. We found that the awake state was close to the bifurcation point between locally and globally dominated synchronization in both human and monkey data. As subjects lost consciousness, the alpha values dropped progressively with deeper levels of sleep or anesthesia, indicating a gradual shift in the dynamics towards smaller synchronization events (Figs. 2C-F). These results suggest that changes in global excitability are the main determinant of different levels of large-scale synchronization in the simulated and empirical data.

Model predictions

The present findings demonstrate that the model can mirror the time-varying properties of global versus local synchronization across different levels of consciousness. We therefore tested, whether the simulations can also correctly predict the change of other metrics across vigilance states. First, we calculated the grand-average functional connectivity (FC) of fMRI signals for each state of the empirical and model data. In accordance with previous findings (Barttfeld et al., 2015), average FC between brain areas was highest in the awake state and significantly decreased with onset and progression into deeper levels of unconsciousness in both human and monkey data (Fig. 3A, left, one-way rm-ANOVA: $F3,51 = 0.99*10^3$, $p < 0.0001$, $\varepsilon = 0.42$ in the human and $F2,28 = 1.81 * 10^3$, $p < 0.0001$, $\varepsilon = 0.78$ in the monkey; ; posthoc test: $p < 0.001$ for all pairs). Importantly, the model also showed higher average FC during the awake state and lowest FC during the most profound levels of unconsciousness (Fig. 3A, right). Next, we examined the relationship between structural (SC) and functional connectivity, which has been shown to undergo changes across consciousness states (Barttfeld et al., 2015; Tagliazucchi

et al., 2016b). Similarly, we detected an increase of the SC-FC relation with loss of consciousness as compared to the awake state. This indicates that in the unconscious states the direct anatomical connections, whereas in the awake state further network effects emerge beyond pair-wise interactions (Fig. 3B, left, one-way rm-ANOVA: $F_{3,51} = 1.13 * 10^3$, $p <$ 0.0001, $\varepsilon = 0.45$ in the human and $F_{2,18} = 2.56 * 10^3$, $p < 0.0001$, $\varepsilon = 0.92$ in the monkey; ; posthoc test: $p < 0.001$ for all pairs). Again, the model correctly reproduced the behavior of the SC-FC relationship for different levels of consciousness (Fig. 3B, right). Other descriptors that are used to characterize consciousness include the level of integration and segregation, which are in general inversely related (Deco et al., 2015). Integrated activity is characterized by synchronization across multiple brain areas while modularity refers to the prevalence of locally confined processing. In the human and monkey data, integration significantly increased, as brain activity approaches wakefulness (Fig. 3C, left, one-way rm-ANOVA: $F_{3,51} = 0.91 * 10^3$, $p <$ 0.0001, $\varepsilon = 0.43$ in the human and $F_{2,28} = 4.36 * 10^3$, $p < 0.0001$, $\varepsilon = 0.84$ in the monkey; ; posthoc test: $p < 0.001$ for all pairs) due to rising levels of brain-wide synchronization. In contrast, local activation dominated during unconscious states with more segregation, as quantified by the modularity value obtained for the optimal partition when breaking the FC matrix into clusters (Fig. 3D, left, one-way rm-ANOVA: $F_{3,51} = 1.04 * 10^3$, $p < 0.0001$, $\varepsilon =$ 0.65 in the human and $F_{2,28} = 4.92 * 10^3$, $p < 0.0001$, $\varepsilon = 0.59$ in the monkey; ; posthoc test: $p < 0.001$ for all pairs). The model correctly predicted the changes of integration and modularity across vigilance states (Figs. 3C, D, right).
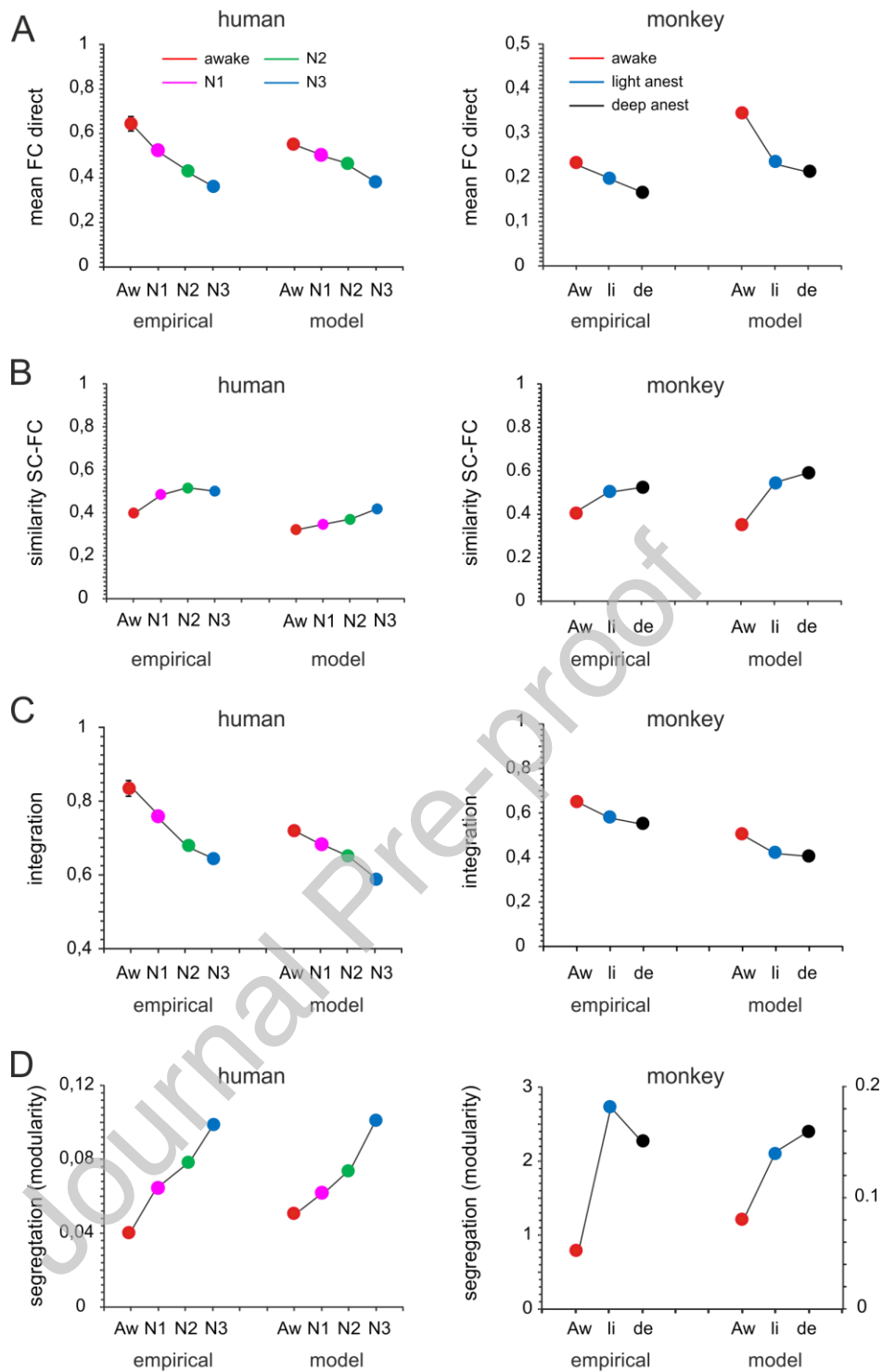
Figure 3. Comparison between empirical data and model predictions for various measures and across different consciousness levels. (A) Mean (±SD) direct FC for empirical and modeled human (left) and monkey data (right) of different consciousness conditions. (B) Same as in (A) for SC-FC similiarity. (C). Same as in (A) for the level of integration. (D) Same as in (A) for the level of functional segregation as measured by modularity.

Analysis of different synchronization states

Previous studies have highlighted that different consciousness levels can be characterized by the relative prevalence of different functional connectivity states (Barttfeld et al., 2015; Demertzi et al., n.d.) with varying levels of fMRI signal correlations and SC-FC relationship. Here, we hypothesize that these states reflect different levels of large-scale synchronization with a frequency of occurrence that is determined by the level of consciousness. To test this hypothesis we split the data into short bins (size = 5 TR) and concatenated bins with similar Fano factor values, representing similar global synchronization levels, into a new dataset. The FF range was chosen to be $1+n <$ FF $< 5+n$, with n being incremented by one for each new dataset. Thus, we obtained datasets with increasing large-scale synchronization, each of which was considered a different state. This procedure was repeated for both empirical and model data for each vigilance state.

We first examined how the average amplitude of the fMRI signal, measured as the mean z-score of positive peak amplitude, changed across different synchronization states for each vigilance state. The analysis of the human data showed that the BOLD amplitude steadily rises as global synchronization increases, indicating that large scale synchronization is associated with stronger local signals (Fig. 4A, left). Importantly, these results were accurately predicted by the model. A similar behavior was found in the empirical and modeled monkey data for the awake state, while the fMRI signal amplitude slightly dropped with stronger synchronization in the two anesthetized states of the empirical data (Fig. 4A, right).

Next, we studied how the mean FC evolves across the different synchronization states. As the global synchronization increased in the empirical human data, the mean FC also grew stronger for all vigilance conditions (Fig. 4B, left). However, the mean FC for most large-scale synchronization states was higher in the awake state as compared to the unconscious conditions. Likewise, highly synchronized states also showed the highest FC and were only found in the awake condition. The model was able to replicate the empirical findings. In the empirical and

modeled monkey data, similar results were obtained with more pronounced FC differences between awake and unconscious conditions (Fig. 4B, right).

We then studied to what extent the SC is expressed in the FC as a function of different global synchronization states. We found that with increasing levels of large-scale synchrony, the similarity between empirical FC and SC in humans decreases and reaches minimum values during highly synchronized states prevalent only during the awake condition (Fig. 4C, left). A similar decrease can be seen in the model, even though very small SC-FC correlation values are also found in unconscious states. The same results hold in the monkey data, with the exception that high SC-FC similarity is found predominately in weakly synchronized states during anesthesia (Fig. 4C, right).

The integration measure also increased with rising levels of global synchronization across all consciousness conditions in humans and monkeys, a result that was accurately reproduced by the model (Fig. 4D). In contrast, modularity decreased with large-scale synchrony in human empirical and simulated data (Fig. 4E, left). Interestingly, modularity in the monkey initially decreased with larger FF values and subsequently increased again in the anesthetized states, showing a U-shaped behavior in both empirical and modeled data. In contrast, the awake state was characterized by a monotonic decrease of modularity with higher FF values as seen in humans.

Overall, this analysis suggests that different global synchronization states with varying levels of FC, expression of SC, integration and modularity exist across different vigilance conditions. The level of consciousness can then be distinguished based on the composition of synchronization states, which as the model shows is a function of global excitability levels across the entire brain.
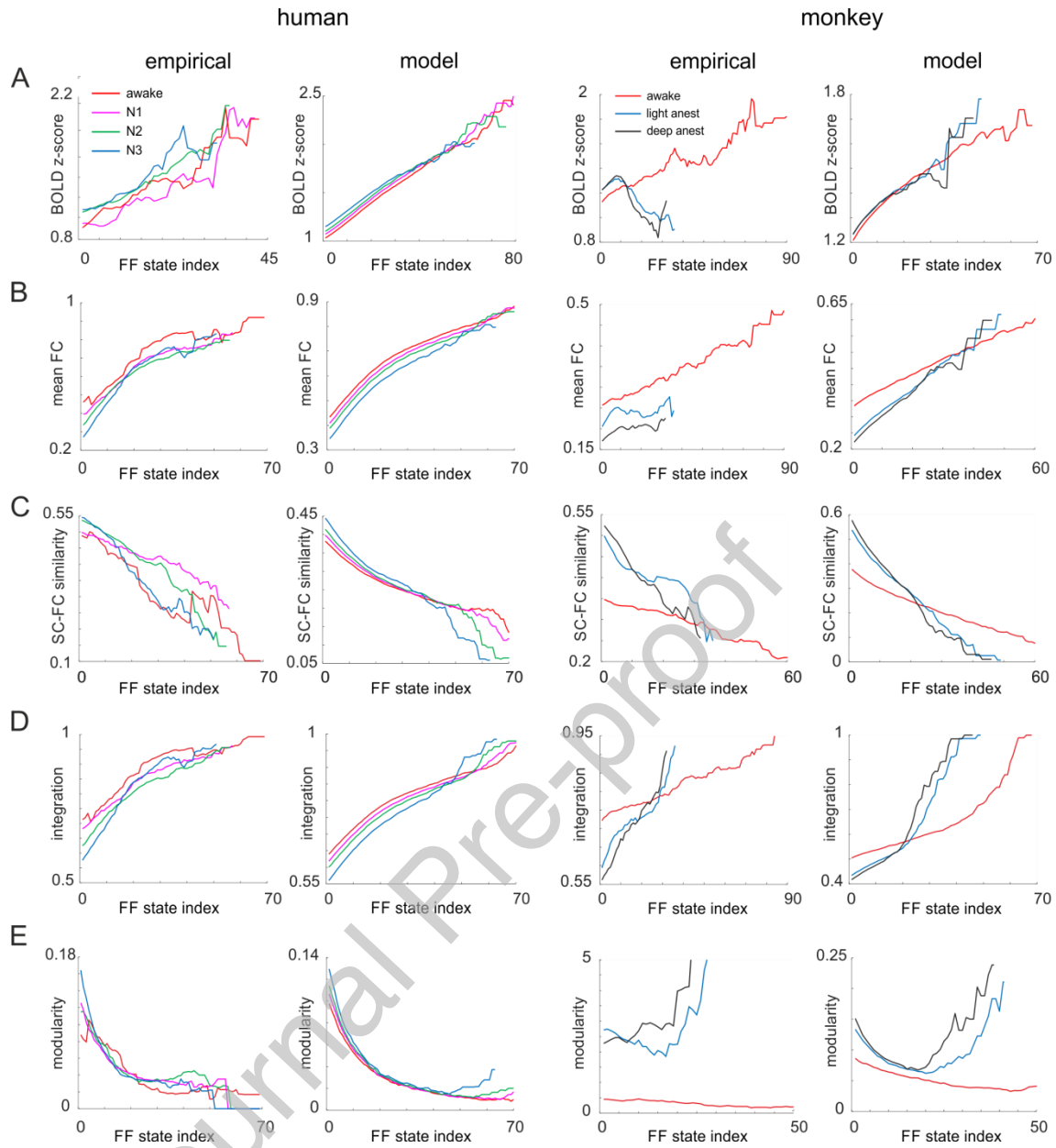
Figure 4. Various metrics change with the level of global synchronization (FF states) across different consciousness conditions. (A) Average peak amplitude (z-score) within a time window of 5 TR as a function of FF state in empirical and modeled human (left) and monkey data (right). (B) Mean direct FC as a function of global synchronization states for human and monkey data. (C) SC-FC similarity for different global synchronization states in humans and monkeys. (D-E) Same as in (C) for integration and modularity, respectively.

Single trial analysis

The previous results were obtained by computing synchronization metrics from data merged across all trials and subjects of a consciousness state. To test whether the composition of synchronization states can also delineate consciousness states at the single-trial level, we computed FF distributions and the other FC-based metric for each trial separately. In humans, we recorded one trial per consciousness state with a duration that ranged between ~90 and 1000 TR (see Supplementary Fig.4 for details). We found significant beta value differences between the awake state and unconscious states (N2 and/or N3) (one-way rm-ANOVA: $F_{3,51} = 5.7$, $p < 0.002$, $\varepsilon = 0.93$) which was repeated for the other measures except modularity, while the separation between unconscious states was not consistent across sleep stages (Fig 5A, Supplementary Fig. 5). Moreover, when comparing consciousness states within single subjects, there was a monotonic decrease of beta values from the awake state to N3 sleep only in a few cases, while most subjects did not show a consistent change of beta across consciousness states (Supplementary Fig. 6). Notably, the beta values and other measures were highly overlapping across states, prohibiting an unambiguous identification of consciousness states. As we have shown above, each consciousness state can be defined by a distribution of synchronization events, in which reduced global synchrony occurs across all states, while larger events are mainly prevalent during the awake state and N1 sleep. Thus, disambiguation of states requires sufficient sampling to provide accurate statistics, which may not be the case in our single trial analysis due to their short duration.

To test whether these findings can be replicated by the model, we simulated several short trials (250 TR) and averaged across trials (Fig. 5B). Similar to the empirical counterpart, the beta values monotonically decreased with the depth of sleep with statistical differences across states as seen in the empirical data, while they remained highly overlapping. In contrast, when we performed simulations with long trials (10000 TR), the overlap disappeared and each trial could be unequivocally assigned to a particular consciousness state (Fig. 5C).

In monkeys, where the trial duration was fixed at 500 TR, the awake state was significantly different from the two unconscious states for all measures (Fig. 5D, Supplementary Fig. 5, one-way rm-ANOVA: $F_{2,60} = 8.6$, $p < 0.0001$, $\varepsilon = 0.45$ in the human and $F_{2,18} = 2.56 * 10^3$, $p < 0.0001$, $\varepsilon = 0.6$ in the monkey). Yet, the values were overlapping between the states, which we reproduced in simulations with short trials (500 TR, Fig., 5E). Similar to humans, the overlap vanished with longer trials (Fig. 5F).

Overall, these results suggest that short trials are less suited for an unambiguous separation of different consciousness states due to insufficient sampling of the synchronization event across time.
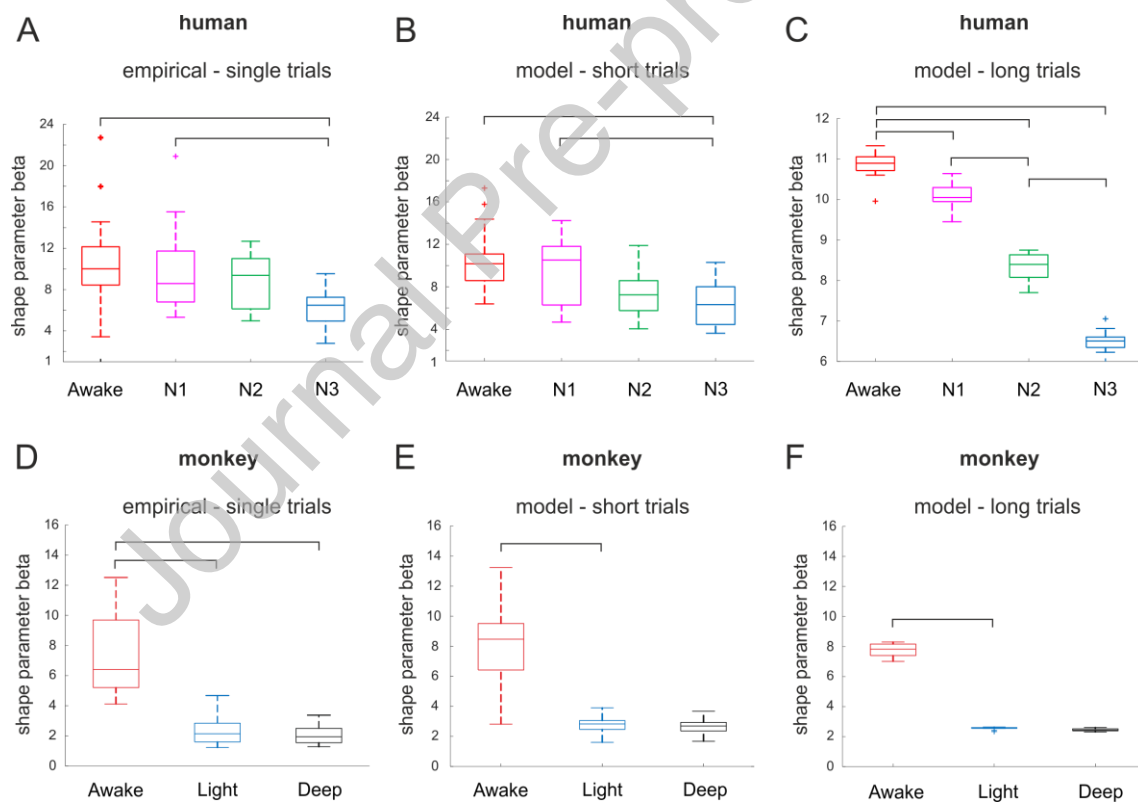

Figure 5. Beta values of the FF distribution for single trials (A) Boxplot (median, 25th and 75th percentile) for beta of single trials across consciousness states in humans. Horizontal bars represent statistical significance (p-value < 0.05). (B) Same (A) for human model simulations with short trials (250 TR). (C) Boxplot for human model simulations with long trials (10000 TR). (D-F) Empirical and model beta values for short and long trials as in the human data.

Model lesions and global synchronization

The correspondence between measures of the empirical and model data suggests that the model may be a viable tool to investigate the impact of specific brain areas on consciousness. We thus employed a lesion approach in which the excitability (i.e. the bifurcation parameter) of individual nodes in the model was strongly reduced mimicking damage after stroke or mechanical trauma (Adhikari et al., 2017). To quantify the consequences of node damage on model dynamics and its associated level of consciousness in the empirical data, we introduce a lesion index (λ) which indicates the loss of global synchronization in the simulations with respect to the synchronization level seen in the awake state of the empirical recording (see Methods for details). A value of 1 reflects model synchronization equivalent to the awake data, while we consider $\lambda < 0.85$ as equal to loss of consciousness.
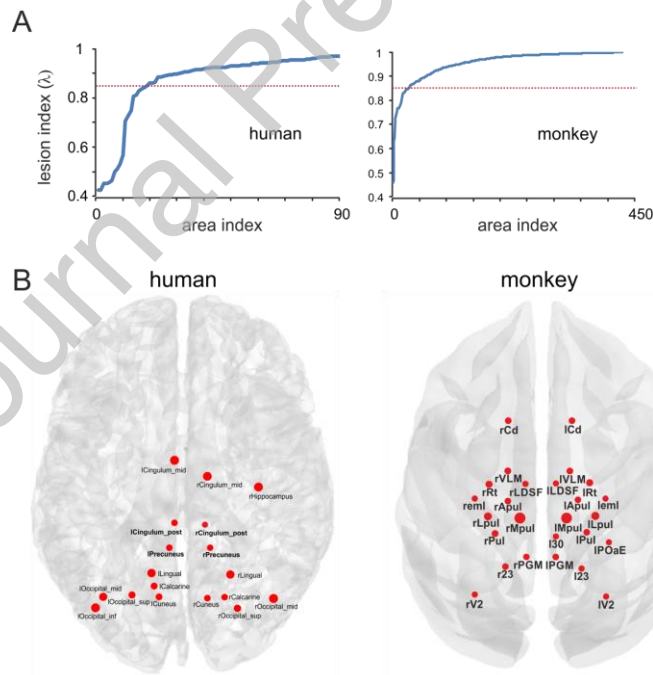
Figure 6. Global synchronization changes after model lesions of specific brain areas. (A) The lesion index (λ) indicates the degree of global synchronization with respect to the awake state (normalized to 1) after the lesion of individual model nodes (abscissa). Dashed red line: threshold for global synchronization levels comparable to conscious (above line) and unconscious states (below line). (B) Brain areas (red circles) that cause a drop below the

red line in (A) after lesion. Circle diameter is scaled to the value of the lesion index of a given area. See Supplementary Tables1-2 for full labels.

When each area was lesioned separately, the impact on large-scale synchronization was modest for most regions and yielded a lesion index that remained above the threshold for dynamics associated with consciousness in both human and monkey data (Fig. 6A). However, the lesion of a few areas strongly reduced brain-wide synchronization with λ reaching values ~0.4 in some cases. In humans these areas were all found in the posterior brain, with the precuneus and posterior cingulate cortex having the most pronounced effect (Fig. 6B, left panel). This is in striking congruence with previous experimental findings pinpointing at a posterior hotspot for consciousness (Koch et al., 2016). Notably, in simulations of monkey data the strongest influence on global synchronization was also found in the posterior cingulate cortex (area 23) and the precuneus (area PGM) together with subcortical nuclei, in particular higher order thalamic nuclei (Fig. 6B, right panel), which in empirical studies play an important role in modulating consciousness (Schiff, 2008)

To gain a better understanding of how these nodes contribute to global dynamics and putatively to the maintenance of consciousness, we conducted a graph theoretical analysis of the human and monkey structural connectomes. We first tested the structural matrices for the presence of a rich club, i.e. network hubs that are highly interconnected with other brain areas and also strongly linked between themselves. Based on the k-density metric (see Methods, Supplementary Fig.7), we found several rich club nodes in the human, including the precuneus and posterior cingulate cortex, and monkey connectome, which were mainly located in subcortical nuclei and area PMG (precuneus) (Figs. 7A-B, asterisks). Even though a majority of these areas had a strong impact on the level of large-scale synchronization, a large number of brain regions with a low lesion index did not belong to the rich club network (Figs. 6B and 7A-B). We thus searched for a metric that would better reflect the role of each node in maintaining brain-wide synchronization and the awake state. The node communicability, a measure that

captures the propagation of activity across the network after the stimulation of a given node, proved to be a good predictor of synchronization levels (Figs.7A-B). In general, areas with a low lesion index typically also had low communicability values in human and monkey datasets. Surprisingly however, in humans we found two separate linear relationships between communicability and lesion index, one with a steep slope where the impact of lesion was high and another with a shallower slope. We hypothesized that this finding is rooted in the difference of node communicability between different hemispheres, since taking out a node in one hemisphere influences large-scale synchronization both ipsilaterally and contralaterally only if strong interhemispheric connections exist. Thus, a node may have strong communicability in the presence of only ipsilateral connections, but a lower impact on large-scale synchronization, as its activity does not spread to the other hemisphere. We thus calculated communicability separately for each hemisphere and quantified the asymmetry between both communicability values. A value of ~1 indicates high asymmetry with a node exclusively impacting activity in one hemisphere, while asymmetry ~ 0 indicates a strong propagation within both hemispheres. We indeed found that high communicability areas can show different degrees of asymmetry across the two hemispheres (Supplementary Fig. 8). Despite their similar communicability, areas with reduced asymmetry such as the precuneus and posterior cingulate cortex influence brain-wide synchronization strongly, while other nodes with very high asymmetry such as the putamen influence synchronization primarily in one hemisphere with an attenuated impact on brain-wide synchrony (Fig. 7C).
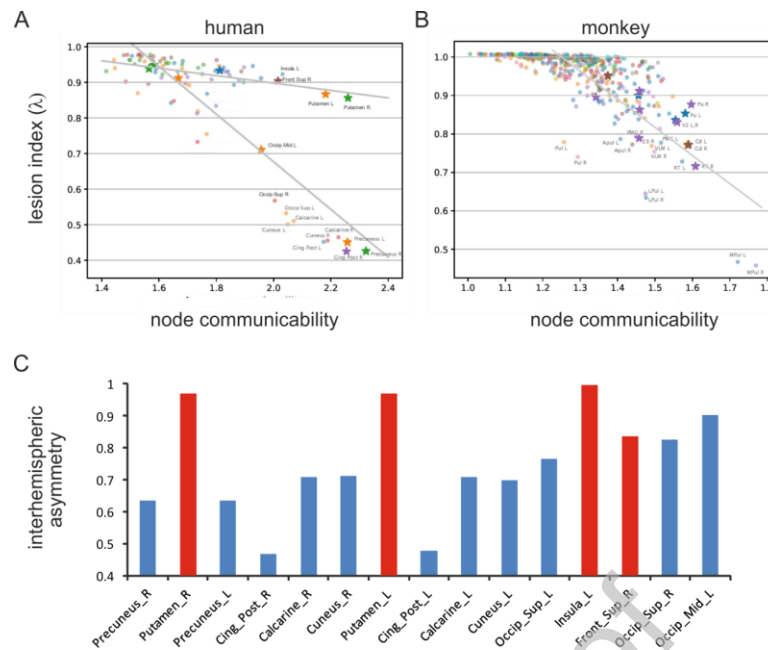
Figure 7. Graph-theoretical properties determine impact of nodes on global synchronization. (A) The lesion index (λ) for each brain area in the human dataset is shown as a function of node communicability computed from the SC matrix. Asterisks indicate brain areas with rich club properties. Straight lines reflect regression lines calculated for two different sets of areas. (B) Same as in A for the monkey dataset. (C) Asymmetry of node communicability computed for each hemisphere separately for the areas of the human connectome with high communicability labeled in (A). Blue bars denote areas falling in the steep slope set, red bars for areas in the shallow slope set.

Discussion

Here, we have shown that the pattern of large-scale synchronization across the brain is a new signature of consciousness and can readily distinguish different consciousness conditions separating awake from unconscious states in human and monkey fMRI data. It separates awake from unconscious conditions and separates various degrees of non-REM sleep and propofol anesthesia. Changes in brain-wide synchrony are accompanied by alterations of other measures of consciousness such as FC, the SC-FC relationship, integration and modularity. Strikingly, the statistics of these metrics were accurately reproduced by a whole-brain model and explained by different global excitability levels that naturally generate different configurations of large-scale synchrony. Additionally, graph theoretical analyses together with model lesion simulations show that the anatomical properties of specific brain areas in the posterior brain play a crucial role in maintaining the level of large-scale synchronization typical of the awake state.

The existence of brain-wide synchronization in fMRI data naturally raises the question whether it reflects a physiological signal (Scholvinck et al., 2010) or should be considered as an artifact caused by e.g. head movements that are usually regressed out(Liu et al., 2017), as was also done here. However, recent studies have demonstrated that large-scale synchrony of fMRI signals not only respect precisely orchestrated electrophysiological changes (Liu et al., 2018a, 2015), but is also tightly linked to acetylcholine release of the basal forebrain, as its lesion abolishes large-scale synchrony (Turchi et al., 2018). Changes in brain-wide synchrony were also found in schizophrenia (Hahamy et al., 2014; Yang et al., 2014). Moreover, the fMRI signal shows wave like propagation (Majeed et al., 2011; Mitra et al., 2014, 2015a) across the entire brain during the awake state with large-scale synchronization (Mitra et al., 2015b), while waves remain confined to specific resting state networks during slow-wave sleep (Mitra et al., 2015b). Lastly, both empirical and model distributions decay exponentially and lack a peak at their tail, where highly widespread synchrony due to artifacts would be expected.

Previous studies have highlighted that fMRI signal synchronization between brain fluctuate overtime, creating different functional connectivity states (Barttfeld et al., 2015; Keilholz et al., 2017). These FC states are tied to different levels of modularity (Betzel et al., 2016; Fukushima et al., 2018a), integration (Shine et al., 2016), varying SC-FC relationships (Barttfeld et al., 2015; Fukushima et al., 2018b), behavior (Shine et al., 2016) and the level of consciousness (Barttfeld et al., 2015; Demertzi et al., 2019). Here, we show that also large-scale synchronization evolves at a fine-grained temporal scale and changes strength across a wide range in the awake state and a largely reduced range during unconscious conditions in both empirical and modeled human and monkey data. We show that global synchrony is related with other measures such as mean FC strength, SC-FC relationship, modularity and integration. These metrics move along a continuum with a range that changes with the consciousness level, rather than reflecting a few discrete states that are correlated with behavior (Shine et al., 2016; Wang et al., 2016). During the awake state, consciousness is maintained over a large range of synchronization states including those that are primarily seen during loss of consciousness with

a lack of global synchrony. Such absence of global synchrony, which we found to dominate during the N3 state, is also consistent with reports that during sleep both the BOLD signal and slow waves/spindles in electrophysiological recordings propagate only locally (Mitra et al., 2015b; Nir et al., 2011; Vyazovskiy et al., 2011). The temporary absence of large-scale synchrony and integration may indicate a low arousal state with drowsiness which is not yet low enough to suppress consciousness, even though a clear correlation with microsleep was not found (Demertzi et al., 2019). On the other hand, highly integrated states have been associated with accurate task performance (Shine et al., 2016) and are predicted by both the integrated information and global neuronal workspace theories of consciousness (Dehaene and Changeux, 2011; Tononi et al., 2016), as conscious processing would require large-scale integration and spread of neuronal activity ('ignition') (Deco et al., 2017b; van Vugt et al., 2018). In contrast, other studies suggest that such strong global synchrony is accompanied by a drop of arousal as defined by a drop in alpha activity and enhanced delta/theta oscillations in simultaneously recorded electrophysiological recordings (Chang et al., 2016; Wong et al., 2013), which is reversed by alertness-promoting caffeine (Wong et al., 2013), and putatively caused by reduced ACH concentrations after a large-scale synchronization event (Liu et al., 2018b). It is possible that such strong synchronization across the brain with high Fano factors reduces functional differentiation of neuronal activity, another hypothesized prerequisite for consciousness (Naci et al., 2018; Tononi et al., 2016). Even though systems close to a bifurcation, as seen in our study for the awake state, theoretically maximize their number of possible states (Shew et al., 2011; Shew and Plenz, 2013), the occasional undifferentiated and more homogeneous activation of large part of the brain would thus diminish alertness. A key component of enhanced differentiation during the awake state might be enhanced inhibition (Rudolph et al., 2007), which allows competition between different neuronal representations and fine-grained activity patterns. Indeed, active suppression of activity has been only found during the awake state, as evidence by a specific FC configuration, containing strong correlation and anticorrelations between specific brain areas (Barttfeld et al., 2015; Demertzi et al., 2019; Fox et al., 2005; Wong et al., 2013). A possible scenario is that such inhibition is reduced during strong global

synchrony, which triggers a large-scale propagation of excitation with lower levels of differentiation. An important limitation of our marker is that the global synchronization index is not sensitive to anticorrelations. Likewise, the presented model does not incorporate mutual inhibition between brain areas and can thus not reproduce the anticorrelated FC states seen during the awake state, a problem which will be addressed in future studies.

Another limitation of our marker of consciousness is that it is based on a distribution which requires sufficient sampling across time to give a robust separation of consciousness states. If sampling is too short the estimation of distribution parameters is inaccurate and consciousness states can have similar marker values, as shown by our single-trial analysis. Yet, our model results suggest that with sufficient recording time states can be distinguished with high fidelity. In addition, the existence of distributions of synchronization strength, which differ in its tail of large-scale synchronization across consciousness states but otherwise overlap in terms of small-scale synchronization, imply that in both conscious and unconscious states there are epochs of neuronal activity in parcellated fMRI data, which are statistically not distinguishable. Thus, more research is needed to overcome this limitation of distribution-based markers and correctly detect consciousness at any given moment in time.

What is the origin of the fluctuations in large-scale synchrony, integration and separation seen in empirical data (Deco et al., 2015; Fukushima and Sporns, 2018) ? There are two scenarios: First, the cortex inherits excitability fluctuations originating in neuromodulatory nuclei or second, fluctuations are created intrinsically in the cortex.

Our whole-brain model creates fluctuations intrinsically and can faithfully the statistics of global synchronization and connectivity measures at a fine temporal scale given a fixed level of global excitability and across a variety of consciousness conditions. Such fluctuations within a continuum of largely synchronized and desynchronized states is an expected property of a dynamical system set close to a Hopf bifurcation point (Jobst et al., 2017), which resembles the awake state in humans and monkeys. This idea is similar to the concept of criticality and

neuronal avalanches (Beggs and Plenz, 2003; Hahn et al., 2017, 2010; Liang et al., 2020; Shew and Plenz, 2013), where a system poised to the critical point generates fluctuations at various spatial scales with occasional avalanches that spread across the entire system, akin to the fMRI waves seen in awake humans (Mitra et al., 2015a). Moving away from the bifurcation or to the subcritical regime by reducing global excitability levels reduces the size of fluctuations and avalanches are restricted to local propagation within well connected resting state networks (Tagliazucchi et al., 2016a). Our model indeed suggests that the transition from awake into deeper stages of sleep or anesthesia is linked to a gradual decrease in global excitability and large-scale functional connectivity.

However, there is also experimental evidence that the variability of cortical connectivity is at least partly driven by changes in neuromodulation. One study showed that cognitive task and integrated FC states were accompanied by dilations of pupil diameter indicative of enhanced activity of subcortical neuromodulator nuclei, in particular the noradrenergic locus coeruleus (Shine et al., 2016). Another study linked the occurrence of global synchronization during resting state to a decrease in cholinergic basal forebrain activity suggesting that a decreased ACH tone is causally related to widespread propagation of neuronal activity (Liu et al., 2018a). Furthermore, inactivation of the nucleus basalis disrupts the presence of large-scale synchronization, while keeping the structure of local resting state network synchronization intact (Turchi et al., 2018). This finding is reminiscent of our model result where reduced global excitability diminished global synchrony. Thus, it remains to be studied how fluctuations in neuromodulation are causally related to individual connectivity and synchronization states. It is unclear to what extent neuromodulatory changes are stochastic and independent of cortical activity or are at least partly under control of cortical dynamics.

Our whole-brain modeling also allowed us to mimick lesions of individual areas due to e.g. stroke, and studied their effect on global synchrony as seen during the awake state. We found a few key areas that are crucial for maintaining the model in a condition akin to the awake state and their damage resulted in a transition into model dynamics in which brain-wide

synchronization events were absent similar to unconscious states. Surprisingly, these areas were located in the back of the brain, centered around the 'posterior hotspot' of consciousness described in the literature (Boly et al., 2017; Koch et al., 2016; Tagliazucchi, 2017; Vogt and Laureys, 2005). The most influential areas in the model were the precuneus and posterior cingulate cortex in both humans and monkeys, which have been previously found to be key areas in maintaining consciousness (Alkire et al., 2008; Cavanna, 2007). In the monkey thalamic nuclei had a large impact,as described previously in empirical studies (Schiff, 2008). In the human parcellation the thalamus was only represented by one node per hemisphere with less impact on consciousness, explained by its weaker node communicability of the anatomical connections as compared to highly influential areas (Fig. 7A). Using graph theoretical analysis we identified a few areas with large impact on large-scale synchrony are part of the structural rich-club, a highly interconnected network of hubs that are part of the default node network in the posterior brain (van den Heuvel and Sporns, 2011; Zamora-López et al., 2011, 2010). More generally, the effect of individual brain areas on global synchronization was attributed to the degree of node communicability, i.e. how strongly activity initiated in a given area propagates across the brain. We also found that strong interhemispheric connections play a crucial role in mediating synchrony across the entire brain. This effect was most pronounced in humans and much less in monkeys. We can only speculate about the causes for this difference between species. Aside from existing anatomical differences, it is also conceivable that the difference in parcellation or tractography, which is known to confound interhemispheric connections specifically, may play a role. Overall, these results demonstrate that excitability and information transfer through single nodes is not only determined by neuromodulation, but also by the activity flowing into and out of crucial nodes in the network. These nodes then play a paramount role in keeping overall global excitability at a level necessary for conscious processing.

In conclusion, we described a novel marker for different consciousness states that is based on large-scale synchronization of the fMRI signal across the brain and solidly explained by

changes of global excitability in a whole brain model. This model also suggests that the maintenance of consciousness is also dependent on graph theoretical properties of individual brain areas making conscious experience vulnerable to lesion of specific nodes.

Methods

Human study

Participants: For this study, approved by the local ethics committee, we collected data from 63 young healthy subjects, who provided written informed consent and were reimbursed for their participation. Eight subjects remained awake during scanning and were not included in the study, leaving five subjects who reached at least N1 sleep (36 females, mean±SD age of 23.4 ± 3.3 years). Simultaneous EEG-fMRI was recorded in the evening after a regular sleeping schedule. For this study, we only included 18 participants, who went through all three sleep stages (N1, N2 and N3).

Acquisition of fMRI and EEG and artifact processing: We simultaneously recorded EEG via a cap (modified BrainCapMR, Easycap) and fMRI (1505 volumes of T2*-weighted echo planar images, TR/TE = 2080 ms/30 ms, matrix 64 x 64, voxel size 3 x 3 x 2 mm^3, distance factor 50%; FOV 192 mm^2) with a 3T Siemens Trio scanner. Polysomnography was performed, recording chin and tibial EMG, ECG, EOG bipolarly (sampling rate 5 kHz, low pass filter 1 kHz) and EEG with 30 channels using FCz as the reference (sampling rate 5 kHz, low pass filter 250 Hz); We recorded pulse oxymetry and respiration with sensors from the Trio (sampling rate 50 Hz) and MR scanner compatible devices (BrainAmpMR+, BrainAmpExG; Brain Products), which aided sleep scoring during fMRI recordings (Jahnke et al., 2012) (AASM, 2007). MRI and pulse artifacts were removed with the average artifact subtraction (AAS) method(Allen et al., 1998) as implemented in Vision Analyzer2 (Brain Products) and thereafter by objective (CBC parameters, Vision Analyzer) ICA-based rejection of residual artifact components, after which the EEG had a sampling rate of 250 Hz (Jahnke et al., 2012) . Likewise, motion artifacts

in the EEG were removed based on ICA using the Vision Analyzer2 software. An expert scored sleep stages manually according to the AASM criteria (AASM, 2007).

fMRI preprocessing: Using Echo planar imaging (EPI) data were realigned, normalized (MNI space), spatially smoothed (Gaussian kernel, 8-mm^3 full width at half maximum) with the Statistical Parametric Mapping software (SPM8, www. fil.ion.ucl.ac.uk/spm) and resampled to a 4 x 4 x 4 mm^3 resolution for artifact removal. Then we regressed out cardiac, respiratory (both estimated using the RETROICOR method(Glover et al., 2000)) and motion-induced noise. For data analysis, the data were first bandpass filtered in the range of 0.01-0.1 Hz (Cordes et al., 2001) using a second order Butterworth filter or between 0.07 and 0.09 Hz to compare empirical with model data (see below). All voxels were then projected onto the automated anatomic labeling (AAL) atlas (Tzourio-Mazoyer et al., 2002) (90 areas, 76 cortical regions, 14 subcortical regions, excluding cerebellar regions, Supplementary Table 1) by averaging their time courses within each AAL cluster. Alternatively, we also computed the first principal component of the voxel time-series and compared it with the averaged time course. The results show that the two time series are highly similar (Supplementary Fig. 1A) with a correlation coefficient of 0.96 ± 0.04 (Supplementary Fig. 1B).

Anatomical dataset acquisition in humans with DTI: The human SC-matrix was obtained at Aarhus University, Denmark using DTI (3T Siemens Skyra scanner) in 16 healthy right-handed participants (11 men and five women, mean age: 24.75 ± 2.54). Subjects with a history of psychiatric or neurologic disorders were not included in this study. The T1 acquisition of the structural MRI was performed with a voxel size of 1 mm^3, a reconstructed matrix size of 256 x 256, echo time (TE) of 3.8 ms and repetition time (TR) of 2300 ms. The DTI data were acquired using TR = 9000 ms, TE = 84 ms, flip angle = 90°, reconstructed matrix size of 106 x 106, voxel size of 1.98 x 1.98 mm with slice thickness of 2 mm and a bandwidth of 1745 Hz/Px. Moreover, the data collection was carried out with 62 optimal nonlinear diffusion gradient directions at b=1500 s/mm^2 and roughly one nondiffusion weighted image (DWI; b = 0) per 10 diffusion-weighted images was obtained. In addition, DTI images were taken with opposing

phase encoding directions (anterior to posterior or posterior to anterior). Similar to the fMRI data, we parcellated the structural scans into 90 areas using the AAL template. We used the linear registration tool from the FSL toolbox (www.fmrib.ox. ac.uk/fsl, FMRIB(Jenkinson et al., 2002)) to coregister the EPI image to the T1-weighted structural image. The T1-weighted image was coregistered to the T1 template of ICBM152 in MNI space(Collins et al., 1994). The resulting transformations were concatenated and inversed and further applied to warp the AAL template (Tzourio-Mazoyer et al., 2002) from MNI space to the EPI native space, where interpolation using nearest-neighbor method ensured that the discrete labeling values were preserved. SC maps for each participant using the DTI data were acquired and processed based on the two acquired datasets with different phase encoding. To construct the SC matrix, we estimated connections between nodes defined by the AAL atlas using probabilistic tractography and averaged across subjects.

Monkey study

Animals: Three rhesus macaques (*Macaca mulatta*, 1 male, 2 females, weight 5-8 kg, age 6-12 years), were tested for each arousal state (awake, moderate propofol sedation, deep propofol anesthesia). All procedures were conducted in accordance with the European convention for animal care (86-406) and the National Institutes of Health's Guide for the Care and Use of Laboratory Animals. Macaque studies were approved by the institutional Ethical Committee (protocols #10-003).

Propofol Anesthesia Protocol: Detailed methodology was described in our previous studies (Barttfeld et al, PNAS, 2015; Uhrig et al, Anesthesiology, 2018). The propofol anesthesia levels (moderate and deep anesthesia) were defined using a clinical score, the monkey sedation scale (spontaneous movements, response to juice presentation, shaking/prodding, toe pinch and corneal reflex) determined at the beginning and the end of each scanning session and continuous electroencephalography (EEG) monitoring (Barttfeld et al., 2015; Uhrig et al., 2018). Under deep propofol anesthesia (general anesthesia), monkeys did not respond to any stimuli. EEG

Propofol anesthesia levels were defined as follows (Barttfeld et al., 2015; Uhrig et al., 2018): level 1, awake state, posterior alpha waves and anterior beta waves; level 2, light propofol sedation, increasing of the amplitude of alpha waves and anterior diffusion of alpha waves; level 3, moderate propofol sedation, diffuse and wide alpha waves, and anterior theta waves; level 4, deep propofol anesthesia (general anesthesia), diffuse delta waves, waves of low amplitude and anterior alpha waves (10 Hz); level 5, very deep sedation (deeper then level of general anesthesia), burst suppression.

The awake monkeys were trained to be injected with an intravenous propofol bolus (5-7.5 mg/kg i.v.; Fresenius Kabi, France) to induce anesthesia, followed by target-controlled infusion (Alaris PK Syringe pump, CareFusion, CA, USA) of propofol (moderate propofol sedation: 3.7-4.0 microg/ml; deep propofol anesthesia 5.6-7,2 microg/ml) based on the 'Paedfusor' pharmacokinetic model(Absalom and Kenny, 2005). During moderate propofol sedation sessions, a muscle-blocking agent was co-administered (cisatracrium, 0.15 mg/kg bolus i.v. followed by continuous i.v. infusion at a rate of 0.18 mg/kg/h, GlaxoSmithKline, France) to prevent artifacts related to potential movements during the fMRI acquisition. Monkeys were intubated and ventilated. Heart rate, non-invasive blood pressure, oxygen saturation, respiratory rate, end-tidal CO2, cutaneous temperature was monitored (Maglife, Schiller, France) and recorded online (Schiller, France) (Barttfeld et al., 2015; Uhrig et al., 2018) Temperature, hemodynamic and ventilation parameters were kept constant during each experiment (Barttfeld et al., 2015; Uhrig et al., 2018).

Awake state Protocol for the Monkeys: For the awake state acquisitions, monkeys were implanted with an MR-compatible headpost and trained to sit in the sphinx position in a primate chair (Uhrig et al., 2014; Wang et al., 2015). Monkeys sat in the dark inside the MRI without any task (Barttfeld et al., 2015; Uhrig et al., 2018).

Monkey fMRI acquisition: Monkeys were scanned with a customized single transmit-receiver surface coil on a 3-T horizontal scanner (Siemens Tim Trio, Erlangen, Germany). Before each scanning session, monocrystalline iron oxide nanoparticles (MION, Feraheme; AMAG

Pharmaceuticals; 10 mg/kg, i.v.) were injected into the monkey's saphenous vein(Barttfeld et al., 2015; Uhrig et al., 2018). Each functional scan contained 500 gradient-echoplanar whole-brain images (TR = 2400 ms; TE = 20 ms; and 1.5-mm^3 voxel size;). 27 awake runs, 25 moderate propofol sedation runs and 31 deep propofol anesthesia runs were acquired.

Monkey fMRI preprocessing: Monkey fMRI images were reoriented, realigned and rigidly co-registered to the anatomical template of the monkey Montreal Neurological Institute space (MNI) (Frey et al., 2011; Uhrig et al., 2014). We also regressed out movement parameters resulting from rigid body correction for head motion. We removed the global signal from the images to minimize the potential respiratory and cardiac effects associated with the propofol administration. Voxel time series were parcellated according to the Paxinos atlas(Paxinos et al., 2009) (see Supplementary Table 2), encompassing 432 cortical and subcortical areas. The signals were then band-pass filtered between 0.01 and 0.1 Hz or in the range of 0.07-0.09 Hz to compare empirical with model data (see below).

Anatomical dataset acquisition in monkeys with diffusion tensor imaging (DTI): DTI data collected in 271 young rhesus macaques in the age-range of 0.7370 to 4.2027 years (Adluru et al., 2012) were used for the creation of a macaque SC matrix. Data collection in macaques was performed using protocols approved by the University of Wisconsin Institutional Animal Care and Use Committee (IACUC). Before undergoing MRI acquisition, the monkeys were anesthetized using ketamine (15 mg/kg). MRI scanning was performed using a GE SIGNA 3T scanner. MR scanning was performed using a two-dimensional, echo-planar, diffusion-weighted, spin-echo sequence with the following parameters: repetition time = 10s; echo time = 77.2 ms; field of view=14 cm; matrix=128×128; 2.5 mm thick contiguous slices; echo-planar echo spacing=800 μs. Diffusion imaging (b=1000s/mm^2) was performed in 12 non-collinear directions with one non-diffusion weighted image and the acquisition was repeated six times and averaged. The volumes were eddy-current corrected using FSL and then brain extraction was performed in a semi-automated manner(Adluru et al., 2012). Following spatial normalization of the single-monkey DT images to monkey MNI space(Frey et al., 2011) using

DTI-TK, an advanced DTI spatial normalization tool (http://www.nitrc.org/projects/dtitk), a DTI template was computed as their Log-Euclidean mean. A brain parcellation with 432 distinct areas in MNI space, defined according to the Paxinos atlas (Paxinos et al., 2009) was used for probabilistic tractography(Behrens et al., 2003). Accordingly, an SC matrix, representing the strength of connectivity between pairs of network nodes (i.e., atlas regions) was estimated.

Analysis of global synchronization

For the analysis of global synchronization, we first extracted discrete events from all empirical and modeled data by assigning a time stamp to each positive peak of the z-scored data similar to previous studies (Deco et al., 2017b; Tagliazucchi et al., 2012). As a control we also repeated subsequent analysis on events that were based on negative peak, which yielded the same results (Supp Fig. 1A-B). Next, we chunked the data into sliding windows with different sizes ranging between 5 and 50 TR. The window was advanced in steps of 1TR. To quantify global synchronization, we took advantage of the Fano factor which was used in classical point process analysis to assess the presence of globally synchronized spiking activity in E-I networks (Brunel and Hakim, 1999; Hahn et al., 2017; Kumar et al., 2008). To this end we calculated the sum of all events found within 1 TR of a window, which resulted in a sequence of counts with length equal to the window size. The Fano factor (FF) of the count sequence was then derived based on the following relationship:

$$FF = \frac{var(counts)}{mean(counts)} \quad (1)$$

The value of the Fano factor gives insight into the correlation structure of the events within each time window. FF ~ 1 indicates that all the events appear independently from each other and seem to have been drawn from a random Poisson process. In the presence of large-scale synchronization of events across many brain areas, the FF increases strongly (FF>>1) as the synchrony confines most events now to a short period of time (1-2 TRs) which is followed by a period with only few events due to synchronization of the negative peaks. FFs were computed

for each time window and summarized in a FF distribution. To quantify the overall level of global synchronization, we fitted a Gamma distribution which is defined as follows:

$$N(F, \beta, \theta) = \frac{\theta^{\beta}}{\Gamma(\beta)} \, F^{\beta-1} \, e^{-\theta F} (-\theta F); \quad \beta > 0, \theta > 0 \qquad (2)$$

,where β denotes the shape parameter, θ the scale parameter and Γ represents the gamma function. Subsequently we used the shape parameter β to quantify the level of consciousness by assigning a single number to each condition that reflects the overall level of large-scale synchrony.

For FF = 1, all events are uncorrelated and correspond to a Poisson process (Fig. 1F). Global bursts of events result in higher order correlations and are characterized by a large variance in event counts due to a concentration of events within a few TR followed by TRs with absence of events. As a result, the Fano factor assumes values >> 1 and measures the degree of global synchronization of brain activity across all areas. We obtained the distribution of Fano factors from all windows for each individual of an age group, which were then merged into a single distribution for an entire age group. An exponential function with exponent λ was then fitted to both the model and empirical FF distributions.

Statistical analysis

To test for significant differences between beta values and other metrics across different consciousness conditions at the group level, we applied a jackknife approach and created N datasets (N = number of subjects in humans and trials in monkeys per for a given consciousness level) for each vigilance condition, each time concatenating N-1 subjects/trials and leave one out. The new datasets were then assessed using a one-way repeated measure (rm) ANOVA and posthoc tests with Bonferroni correction. The significance level was set to $p < 0.05$. In case the sphericity (ε) assumption of the rm-ANOVA was violated, as assessed by a Mauchly test, the p-values and degrees of freedom adjusted by the Huynh-Feldt estimate of ε. To compute goodness

of fit for gamma distributions fitted to the Fano factor distributions, we used a one-sample Kolomogorov-Smirnov test.

Functional connectivity

To quantify statistical dependencies between empirical and modeled fMRI time series, we calculated the Pearson correlation coefficients across all brain areas, which were subsequently averaged for each consciousness condition or Fano factor state.

SC-FC relationship

The structure-function relationship for each consciousness condition was assessed by computing the Pearson correlation coefficient between the structural connectivity matrices (human and monkey) and the functional connectivity matrices for different consciousness levels or Fano factor states.

Integration

We use an integration measure based on the largest connected component of the FC matrix, as defined previously (Deco et al., 2015). As a first step, the FC matrix is binarized by setting connections above a threshold θ to 1 and discarding connections below the threshold, which has a range between 0 and 1. We then search for the largest connected subgraph, i.e. the nodes that are connected without further connections to the remaining nodes of the entire matrix. The size of the largest component (i.e. the number of nodes pertaining to the subgraph) is calculated for each θ and integrated across all tested thresholds. To obtain integration values between 0 and 1, the result is normalized by the number of areas N and integration steps. This integration measure is calculated for all consciousness levels and Fano factor states.

Modularity

To quantify to which degree activity during different consciousness levels or Fano factor states is organized in functional communities, we applied the modularity measure of Newman (Newman, 2006). More specifically, this measure gibes insights to what extent an FC matrix can

be broken down into nonoverlapping subnetworks, where the connectivity strength within a group of brain areas is maximized and minimized between different groups. This metric was applied to different consciousness conditions and Fano factor states.

Computational whole-brain model

To study the mechanisms behind global synchronization, we employed a whole-brain model consisting of either 90 nodes, mimicking the parcellation of areas in human data, or 432 nodes corresponding to the empirical monkey parcellation. The modeled brain areas were connected based on the patterns of long-range connections that were extracted by DTI from humans and monkeys. We used the measured fiber density as a proxy for the connectivity strength in the model. To simulate the dynamics of the local fMRI signal we used the normal-form of the Hopf bifurcation (Deco et al., 2017a, 2017b; Hahn et al., 2019), which corresponds to a transition from focus equilibrium with damped, noisy oscillations to limit cycle behavior with self-sustained oscillations similar to networks of excitatory and inhibitory neurons (Brunel, 2000). The dynamics is described by the following set of coupled differential equations:

$$\frac{dx_j}{dt} = \frac{dRe(z_j)}{dt} = \left[a_j\text{-}x_j^2\text{-}y_j^2\right]x_j\text{-}\omega_j y_j + G\sum_i C_{ij}\left(x_i\text{-}x_j\right) + \beta\eta_j(t) \tag{3}$$

$$\frac{dy_j}{dt} = \frac{dIm(z_j)}{dt} = \left[a_j\text{-}x_j^2\text{-}y_j^2\right]y_j + \omega_j x_j + G\sum_i C_{ij}\left(y_i\text{-}y_j\right) + \beta\eta_j(t) \tag{4}$$

, where $\beta\eta_j$ represents additive Gaussian noise with standard deviation $\beta = 0.01$. ω_j is the intrinsic node frequency, which translated to the BOLD frequency f_j via the following expression: $f_j = \frac{\omega_j}{2\pi}$. The BOLD frequency for each model node was set to 0.085 Hz and filtered between 0.075 and 0.095 Hz in the human data simulations or to 0.04 Hz in the monkey model with filtering between 0.03 and 0.05 Hz. These filters were necessary to remove high frequency noise imposed by the Gaussian noise and allow comparison with empirical Fano factor distributions. These model frequencies were chosen, since the empirical data filtered around the same frequency bands can reproduce the same Fano factor distributions that are seen with a more broadband filtering (0.01 – 0.1 Hz). The variable x_j was used to model the local fMRI

signal. The parameter G scales each connection in the anatomical connectivity matrix by a constant value which was set to 0.1 in this study. For each consciousness level we performed a simulation of 100 minutes. For the single trial analysis, we simulated 18 trials of 250 TR for each consciousness state of the human model. For the monkey model we simulate 21,26 and 31 trials of 250 TR for the awake, light and deep anesthesia case, respectively. These simulations were compared with ten long trials of a duration of 10000 TR.

In an unconnected node, the dynamical behavior is set by bifurcation parameter a_j, which exhibits a supercritical Hopf bifurcation at $a_j = 0$. This means that the activity transitions from a stable focus equilibrium governed by resonance and noisy oscillations at $a_j < 0$ to a stable limit cycle at $a_j > 0$ with self-sustained oscillations. However, as soon as a node is embedded in a large scale network, the impinging connections change the bifurcation point to negative values. In order to find the a_j for the large-scale anatomical network of the human and monkey DTI data, we took advantage of the fact that the Fano factor distributions (see above) for small window sizes (5 TR), followed an exponential distribution when a_j was set below the bifurcation (Fig. 2B). As soon as $a_j >$ bifurcation, the network produced a global oscillations which was visible as a bump in the FF distribution and thus a deviation of the exponential FF decay. We thus defined the bifurcation point as the value of a_j, where the exponential fit, as assessed by a Kolmogorov-Smirnov distance, increased to values above 0.1 (Fig. 2C). The a_j values at the bifurcation point for the human ($a_j \sim 0.66$) and monkey ($a_j \sim -0.33$) SC matrices where then normalized to zero (Figs 2D-G). To fit the model to the data we performed a grid search to find a_j, where the distance $|\beta_{emp} - \beta_{mod}|$ of the empirical and modeled FF distributions was minimized.

Model lesion analysis

To study the role of individual brain areas for model dynamics and global synchronization we conducted a lesion simulations by setting the bifurcation parameter of single nodes j to a value of $a_j = -2.65$ in humans and $a_j = -1.31$ for monkeys, while keeping the other nodes at values that

correspond to the awake state (-0.663 for humans, -0.329 for monkeys). The impact on global synchronization by a single node lesion was then quantified by the lesion index λ, which we defined as follows:

$$\lambda = \frac{\beta_{awake}}{\beta_{lesion}} \qquad (5)$$

, where β_{awake} represents the beta value of the FF distribution found in the awake state (human or monkey) and β_{lesion} indicates the beta value after the node lesion with a simulation time of 10 minutes. The lesion index λ ranges between 0 and 1, and reflects the fraction of global synchrony after the lesion as compared to the awake state in either monkey or human data models. Thus λ~1 means that the global synchronization are barely affected by the lesion, while λ<<1 is a result of a strong influence of a given node on global dynamics.

Graph theoretical analysis

The SC matrices of human and monkeys were studied using several graph analysis tools. A rich club was identified in both SC networks. Rich-club identification implies the calculation of the *k*-density, a recursive calculation that computes the density of the remaining network after all nodes with degree k' ≤ k have been removed, until no nodes are left (Zamora-López et al., 2010). The case k = 0 corresponds to the density of the original network. If the *k*-density grows with k, it means that the nodes with largest degree are densely interconnected with each other. If the *k*-density decays, it means that the nodes with largest degree are indeed not connected with each other. The two SC networks display a growing k-density function and clearly contain a rich-club, taken as the remaining subset of hubs with node degree k' > 47 in humans and k' > 108 in monkeys.

Communicability (M) is a graph metric that quantifies the "influence" one node exerts over another given the path structure of the network (Estrada and Hatano, 2008). It accounts for the fact that (i) information flows along all possible paths, not only across the shortest ones, and (ii) that shorter paths are more relevant while influence decays with the length of the path

(Bettinardi et al., 2017). Given the adjacency matrix A of the matrix, communicability is defined as the matrix exponential, e^A, which can be decomposed as the power series:

$$C = e^A = \mathbf{1} + A + \frac{A^2}{2!} + \frac{A^3}{3!} + \frac{A^4}{4!} + \cdots,$$

where the powers $(A^n)_{ij}$ represent the number of paths of length n that run from node i to node j. The communicability of every node, taken as the column sum of the matrix C, was then correlated with the lesion index.

The activity during different consciousness levels (or Fano factor states) is organized into functional communities. Therefore, to quantify the level of segregation in the functional connectivity (FC) matrices we performed a community detection procedure on them. Partitioning the networks into clusters was performed using the Louvain method, optimizing the weighted Newman modularity (Newman, 2006). This measure evaluates the "goodness" of the partition, giving insights to what extent the FC matrices can be broken down into nonoverlapping subnetworks. Optimization of modularity implies that the connectivity strength within a group of brain areas is maximized while the strength between different groups is minimized. Thus, modularity provides a quantitative indication of the level of functional segregation in the FC. This metric was applied to different consciousness conditions and Fano factor states.

To quantify the asymmetry of communicability between the two hemispheres, we first computed communicability of a given node for the right (r) and left hemisphere (l) separately and then calculated the asymmetry (S) according to the following expression:

$$S_{rl} = \frac{|M_l - M_r|}{M_l + M_r} \qquad (6)$$

Asymmetry values range between 0 and 1, such that $S_{rl} \sim 1$ indicates full asymmetry and $S_{rl} \sim 0$ complete symmetry.

Acknowledgments

Author contributions

G.H. and G.D. designed the computational study. G.H. and G.Z. analyzed the data. G.H performed the numerical simulations. H.L. designed the EEG-fMRI experiment and with E.T. collected the EEG and BOLD-fMRI human data. M.K. provided the human DTI data. L.U., B.J. collected and preprocessed the monkey fMRI data, and D.M provided the monkey DTI data. G.H wrote the first draft of the paper, which was finalized by all the remaining authors.

Competing financial interests

The authors declare no competing financial interests.

References

Absalom, A., Kenny, G., 2005. "Paedfusor" pharmacokinetic data set. Br. J. Anaesth. 95, 110. doi:10.1093/bja/aei567

Adhikari, M.H., Hacker, C.D., Siegel, J.S., Griffa, A., Hagmann, P., Deco, G., Corbetta, M., 2017. Decreased integration and information capacity in stroke measured by whole brain models of resting state activity. Brain 140, 1068–1085. doi:10.1093/brain/awx021

Adluru, N., Zhang, H., Fox, A.S., Shelton, S.E., Ennis, C.M., Bartosic, A.M., Oler, J.A., Tromp,

D.P.M., Zakszewski, E., Gee, J.C., Kalin, N.H., Alexander, A.L., 2012. A diffusion tensor brain template for Rhesus Macaques. Neuroimage 59, 306–318. doi:10.1016/j.neuroimage.2011.07.029

Alkire, M.T., Hudetz, A.G., Tononi, G., 2008. Consciusness and Anesthesia. Science (80-.). 7, 876–880. doi:10.1126/science.1149213.Consciousness

Allen, P.J., Polizzi, G., Krakow, K., Fish, D.R., Lemieux, L., 1998. Identification of EEG events in the MR scanner: The problem of pulse artifact and a method for its subtraction. Neuroimage 8, 229–239. doi:10.1006/nimg.1998.0361

Barttfeld, P., Uhrig, L., Sitt, J.D., Sigman, M., Jarraya, B., Dehaene, S., 2015. Signature of consciousness in the dynamics of resting-state brain activity. Proc. Natl. Acad. Sci. 112, 201418031. doi:10.1073/pnas.1418031112

Beggs, J., Plenz, D., 2003. Neuronal avalanches in neocortical circuits. J. Neurosci. 23, 11167–77.

Behrens, T.E.J., Woolrich, M.W., Jenkinson, M., Johansen-Berg, H., Nunes, R.G., Clare, S., Matthews, P.M., Brady, J.M., Smith, S.M., 2003. Characterization and Propagation of Uncertainty in Diffusion-Weighted MR Imaging. Magn. Reson. Med. 50, 1077–1088. doi:10.1002/mrm.10609

Bettinardi, R.G., Deco, G., Karlaftis, V.M., Van Hartevelt, T.J., Fernandes, H.M., Kourtzi, Z., Kringelbach, M.L., Zamora-López, G., 2017. How structure sculpts function: Unveiling the contribution of anatomical connectivity to the brain's spontaneous correlation structure. Chaos 27, 047409. doi:10.1063/1.4980099

Betzel, R.F., Fukushima, M., He, Y., Zuo, X.-N., Sporns, O., 2016. Dynamic fluctuations coincide with periods of high and low modularity in resting-state functional brain networks. Neuroimage 127, 287–297. doi:10.1016/j.neuroimage.2015.12.001

Boly, M., Massimini, M., Tsuchiya, N., Postle, B.R., Koch, C., Tononi, G., 2017. Are the Neural Correlates of Consciousness in the Front or in the Back of the Cerebral Cortex? Clinical and Neuroimaging Evidence. J. Neurosci. 37, 9603–9613. doi:10.1523/JNEUROSCI.3218-16.2017

Boly, M., Perlbarg, V., Marrelec, G., Schabus, M., Laureys, S., Doyon, J., Pélégrini-Issac, M., Maquet, P., Benali, H., 2012. Hierarchical clustering of brain activity during human nonrapid eye movement sleep. Proc. Natl. Acad. Sci. U. S. A. 109, 5856–61. doi:10.1073/pnas.1111133109

Boveroux, P., Vanhaudenhuyse, A., Bruno, M.-A., Noirhomme, Q., Lauwick, S., Luxen, A., Degueldre, C., Plenevaux, A., Schnakers, C., Phillips, C., Brichant, J.-F., Bonhomme, V., Maquet, P., Greicius, M.D., Laureys, S., Boly, M., 2010. Breakdown of within- and between-network Resting State Functional Magnetic Resonance Imaging Connectivity during Propofol-induced Loss of Consciousness. Anesthesiology 113, 1038–1053. doi:10.1097/ALN.0b013e3181f697f5

Brunel, N., 2000. Dynamics of sparsely connected networks of excitatory and inhibitory spiking neurons. J. Comput. Neurosci. 8, 183–208.

Brunel, N., Hakim, V., 1999. Fast global oscillations in networks of integrate-and-fire neurons with low firing rates. Neural Comput. 11, 1621–71.

Cavanna, A.E., 2007. The precuneus and consciousness. CNS Spectr. 12, 545–52.

Chang, C., Leopold, D.A., Schölvinck, M.L., Mandelkow, H., Picchioni, D., Liu, X., Ye, F.Q., Turchi, J.N., Duyn, J.H., 2016. Tracking brain arousal fluctuations with fMRI. Proc. Natl. Acad. Sci. 113, 4518–4523. doi:10.1073/pnas.1520613113

Collins, D.L., Neelin, P., Peters, T.M., Evans, A.C., 1994. Automatic 3d intersubject registration of mr volumetric data in standardized talairach space. J. Comput. Assist. Tomogr. 18, 192–205. doi:10.1097/00004728-199403000-00005

Cordes, D., Haughton, V.M., Arfanakis, K., Carew, J.D., Turski, P. a, Moritz, C.H., Quigley, M. a, Meyerand, M.E., 2001. Frequencies contributing to functional connectivity in the cerebral cortex in "resting-state" data. AJNR. Am. J. Neuroradiol. 22, 1326–33.

Deco, G., Kringelbach, M.L., Jirsa, V.K., Ritter, P., 2017a. The dynamics of resting fluctuations in the brain: metastability and its dynamical cortical core. Sci. Rep. 7, 3095. doi:10.1038/s41598-017-03073-5

Deco, G., Tagliazucchi, E., Laufs, H., Sanjuán, A., Kringelbach, M.L., 2017b. Novel Intrinsic Ignition Method Measuring Local-Global Integration Characterizes Wakefulness and Deep Sleep. eneuro 4, ENEURO.0106–17.2017. doi:10.1523/ENEURO.0106-17.2017

Deco, G., Tononi, G., Boly, M., Kringelbach, M.L., 2015. Rethinking segregation and integration: contributions of whole-brain modelling. Nat. Rev. Neurosci. 16, 430–439. doi:10.1038/nrn3963

Dehaene, S., Changeux, J.-P., 2011. Experimental and theoretical approaches to conscious processing. Neuron 70, 200–27. doi:10.1016/j.neuron.2011.03.018

Demertzi, A., Tagliazucchi, E., … S.D.-S., 2019, undefined, n.d. Human consciousness is supported by dynamic complex patterns of brain signal coordination. advances.sciencemag.org.

Demertzi, A., Tagliazucchi, E., Dehaene, S., Deco, G., Barttfeld, P., Raimondo, F., Martial, C., Fernández-Espejo, D., Rohaut, B., Voss, H.U., Schiff, N.D., Owen, A.M., Laureys, S., Naccache, L., Sitt, J.D., 2019. Human consciousness is supported by dynamic complex patterns of brain signal coordination. Sci. Adv. 5. doi:10.1126/sciadv.aat7603

Estrada, E., Hatano, N., 2008. Communicability in complex networks. Phys. Rev. E 77, 036111. doi:10.1103/PhysRevE.77.036111

Fox, M.D., Snyder, A.Z., Vincent, J.L., Corbetta, M., Van Essen, D.C., Raichle, M.E., 2005. The human brain is intrinsically organized into dynamic, anticorrelated functional networks. Proc. Natl. Acad. Sci. U. S. A. 102, 9673–8. doi:10.1073/pnas.0504136102

Frey, S., Pandya, D.N., Chakravarty, M.M., Bailey, L., Petrides, M., Collins, D.L., 2011. An MRI based average macaque monkey stereotaxic atlas and space (MNI monkey space). Neuroimage 55, 1435–42. doi:10.1016/j.neuroimage.2011.01.040

Fukushima, M., Betzel, R.F., He, Y., de Reus, M.A., van den Heuvel, M.P., Zuo, X.-N, Sporns, O., 2018a. Fluctuations between high- and low-modularity topology in time-resolved functional connectivity. Neuroimage 180, 406–416. doi:10.1016/j.neuroimage.2017.08.044

Fukushima, M., Betzel, R.F., He, Y., van den Heuvel, M.P., Zuo, X.N., Sporns, O., 2018b. Structure–function relationships during segregated and integrated network states of human brain functional connectivity. Brain Struct. Funct. 223, 1091–1106. doi:10.1007/s00429-017-1539-3

Fukushima, M., Betzel, R.F., He, Y., van den Heuvel, M.P., Zuo, X.-N., Sporns, O., 2017. Structure–function relationships during segregated and integrated network states of human brain functional connectivity. Brain Struct. Funct. 223, 1091–1106. doi:10.1007/s00429-017-1539-3

Fukushima, M., Sporns, O., 2018. Comparison of fluctuations in global network topology of modeled and empirical brain functional connectivity. PLoS Comput. Biol. 14, e1006497. doi:10.1371/journal.pcbi.1006497

Glover, G.H., Li, T.Q., Ress, D., 2000. Image-based method for retrospective correction of physiological motion effects in fMRI: RETROICOR. Magn. Reson. Med. 44, 162–167. doi:10.1002/1522-2594(200007)44:1<162::AID-MRM23>3.0.CO;2-E

Gosseries, O., Di, H., Laureys, S., Boly, M., 2014. Measuring consciousness in severely damaged brains. Annu. Rev. Neurosci. 37, 457–78. doi:10.1146/annurev-neuro-062012-170339

Hahamy, A., Calhoun, V., Pearlson, G., Harel, M., Stern, N., Attar, F., Malach, R., Salomon, R., 2014. Save the global: global signal connectivity as a tool for studying clinical populations with functional magnetic resonance imaging. Brain Connect. 4, 395–403. doi:10.1089/brain.2014.0244

Hahn, G., Petermann, T., Havenith, M., Yu, S., Singer, W., Plenz, D., Nikolić, D., 2010. Neuronal avalanches in spontaneous activity in vivo. J. Neurophysiol. 104, 3312. doi:10.1152/jn.00953.2009

Hahn, G., Ponce-Alvarez, A., Monier, C., Benvenuti, G., Kumar, A., Chavane, F., Deco, G., Frégnac, Y., 2017. Spontaneous cortical activity is transiently poised close to criticality. PLOS Comput. Biol. 13, e1005543. doi:10.1371/journal.pcbi.1005543

Hahn, G., Skeide, M.A., Mantini, D., Ganzetti, M., Destexhe, A., Friederici, A.D., Deco, G.,

2019. A new computational approach to estimate whole-brain effective connectivity from functional and structural MRI, applied to language development. Sci. Rep. 9, 8479. doi:10.1038/s41598-019-44909-6

Haimovici, A., Tagliazucchi, E., Balenzuela, P., Laufs, H., 2017. On wakefulness fluctuations as a source of BOLD functional connectivity dynamics. Sci. Rep. 7, 5908. doi:10.1038/s41598-017-06389-4

Hobson, J.A., Pace-Schott, E.F., 2002. The cognitive neuroscience of sleep: Neuronal systems, consciousness and learning. Nat. Rev. Neurosci. doi:10.1038/nrn915

Jahnke, K., von Wegner, F., Morzelewski, A., Borisov, S., Maischein, M., Steinmetz, H., Laufs, H., 2012. To wake or not to wake? The two-sided nature of the human K-complex. Neuroimage 59, 1631–1638. doi:10.1016/j.neuroimage.2011.09.013

Jenkinson, M., Bannister, P., Brady, M., Smith, S., 2002. Improved optimization for the robust and accurate linear registration and motion correction of brain images. Neuroimage 17, 825–841. doi:10.1016/S1053-8119(02)91132-8

Jobst, B.M., Hindriks, R., Laufs, H., Tagliazucchi, E., Hahn, G., Ponce-Alvarez, A., Stevner, A.B.A., Kringelbach, M.L., Deco, G., 2017. Increased Stability and Breakdown of Brain Effective Connectivity During Slow-Wave Sleep: Mechanistic Insights from Whole-Brain Computational Modelling. Sci. Rep. 7, 4634. doi:10.1038/s41598-017-04522-x

Keilholz, S., Caballero-Gaudes, C., Bandettini, P., Deco, G., Calhoun, V., 2017. Time-Resolved Resting-State Functional Magnetic Resonance Imaging Analysis: Current Status, Challenges, and New Directions. Brain Connect. 7, 465–481. doi:10.1089/brain.2017.0543

Koch, C., 2018. What Is Consciousness? Nature 557, S8–S12. doi:10.1038/d41586-018-05097-x

Koch, C., Massimini, M., Boly, M., Tononi, G., 2016. Neural correlates of consciousness: progress and problems. Nat. Rev. Neurosci. 17, 307–321. doi:10.1038/nrn.2016.22

Kumar, A., Rotter, S., Aertsen, A., 2008. Conditions for propagating synchronous spiking and asynchronous firing rates in a cortical network model. J. Neurosci. 28, 5268–80. doi:10.1523/JNEUROSCI.2542-07.2008

Liang, J., Zhou, T., Zhou, C., 2020. Hopf Bifurcation in Mean Field Explains Critical Avalanches in Excitation-Inhibition Balanced Neuronal Networks: A Mechanism for Multiscale Variability.

Liu, T.T., Nalci, A., Falahpour, M., 2017. The Global Signal in fMRI: Nuisance or Information? Neuroimage 150, 213. doi:10.1016/J.NEUROIMAGE.2017.02.036

Liu, X., De Zwart, J.A., Schölvinck, M.L., Chang, C., Ye, F.Q., Leopold, D.A., Duyn, J.H., 2018a. Subcortical evidence for a contribution of arousal to fMRI studies of brain activity. Nat. Commun. 9, 1–10. doi:10.1038/s41467-017-02815-3

Liu, X., De Zwart, J.A., Schölvinck, M.L., Chang, C., Ye, F.Q., Leopold, D.A., Duyn, J.H., 2018b. Subcortical evidence for a contribution of arousal to fMRI studies of brain activity. Nat. Commun. 9, 395. doi:10.1038/s41467-017-02815-3

Liu, X., Yanagawa, T., Leopold, D.A., Chang, C., Ishida, H., Fujii, N., Duyn, J.H., 2015. Arousal transitions in sleep, wakefulness, and anesthesia are characterized by an orderly sequence of cortical events. Neuroimage 116, 222–231. doi:10.1016/j.neuroimage.2015.04.003

Majeed, W., Magnuson, M., Hasenkamp, W., Schwarb, H., Schumacher, E.H., Barsalou, L., Keilholz, S.D., 2011. Spatiotemporal dynamics of low frequency BOLD fluctuations in rats and humans. Neuroimage 54, 1140–50. doi:10.1016/j.neuroimage.2010.08.030

Mashour, G.A., Hudetz, A.G., 2018. Neural Correlates of Unconsciousness in Large-Scale Brain Networks. Trends Neurosci. 41, 150–160. doi:10.1016/j.tins.2018.01.003

Mitra, a, Snyder, a Z., Hacker, C.D., Raichle, M.E., 2014. Lag structure in resting-state fMRI. J. Neurophysiol. 111, 2374–91. doi:10.1152/jn.00804.2013

Mitra, A., Snyder, A.Z., Blazey, T., Raichle, M.E., 2015a. Lag threads organize the brain's intrinsic activity. Proc. Natl. Acad. Sci. 112, E2235–E2244. doi:10.1073/pnas.1503960112

Mitra, A., Snyder, A.Z., Tagliazucchi, E., Laufs, H., Raichle, M.E., 2015b. Title : Propagated infra-slow intrinsic brain activity reorganizes across wake and slow wave sleep 2) Department of Neurology , Washington University , St Louis , MO 63110 , USA 3)

Institute for Medical Psychology , Christian-Albrechts-University Kiel ,. Elife 2015, 1–19. doi:10.7554/eLife.10781

Naci, L., Haugg, A., MacDonald, A., Anello, M., Houldin, E., Naqshbandi, S., Gonzalez-Lara, L.E., Arango, M., Harle, C., Cusack, R., Owen, A.M., 2018. Functional diversity of brain networks supports consciousness and verbal intelligence. Sci. Rep. 8, 1–15. doi:10.1038/s41598-018-31525-z

Newman, M.E.J., 2006. Finding community structure in networks using the eigenvectors of matrices. Phys. Rev. E 74, 036104. doi:10.1103/PhysRevE.74.036104

Nir, Y., Staba, R., Andrillon, T., Vyazovskiy, V., Cirelli, C., Fried, I., Tononi, G., 2011. Regional slow waves and spindles in human sleep. Neuron 70, 153–69. doi:10.1016/j.neuron.2011.02.043

Paxinos, G., Huang, X.-F., Petrides, M., Toga, A., 2009. The Rhesus monkey brain : in stereotaxic coordinates. Fac. Heal. Behav. Sci. - Pap.

Rudolph, M., Pospischil, M., Timofeev, I., Destexhe, A., 2007. Inhibition determines membrane potential dynamics and controls action potential generation in awake and sleeping cat cortex. J. Neurosci. 27, 5280–90. doi:10.1523/JNEUROSCI.4652-06.2007

Scammell, T.E., Arrigoni, E., Lipton, J.O., 2017. Neural Circuitry of Wakefulness and Sleep. Neuron 93, 747–765. doi:10.1016/j.neuron.2017.01.014

Schiff, N.D., 2008. Central thalamic contributions to arousal regulation and neurological disorders of consciousness, in: Annals of the New York Academy of Sciences. Blackwell Publishing Inc., pp. 105–118. doi:10.1196/annals.1417.029

Scholvinck, M.L., Maier, A., Ye, F.Q., Duyn, J.H., Leopold, D.A., 2010. Neural basis of global resting-state fMRI activity. Proc. Natl. Acad. Sci. 107, 10238–10243. doi:10.1073/pnas.0913110107

Shew, W., Yang, H., Yu, S., Roy, R., Plenz, D., 2011. Information capacity and transmission are maximized in balanced cortical networks with neuronal avalanches. J. Neurosci. 31, 55–63. doi:10.1523/JNEUROSCI.4637-10.2011

Shew, W.L., Plenz, D., 2013. The functional benefits of criticality in the cortex. Neuroscientist 19, 88–100. doi:10.1177/1073858412445487

Shine, J.M., Bissett, P.G., Bell, P.T., Koyejo, O., Balsters, J.H., Gorgolewski, K.J., Moodie, C.A., Poldrack, R.A., 2016. The Dynamics of Functional Brain Networks: Integrated Network States during Cognitive Task Performance. Neuron 92, 544–554. doi:10.1016/j.neuron.2016.09.018

Spoormaker, V.I., Schroter, M.S., Gleiser, P.M., Andrade, K.C., Dresler, M., Wehrle, R., Samann, P.G., Czisch, M., 2010. Development of a Large-Scale Functional Brain Network during Human Non-Rapid Eye Movement Sleep. J. Neurosci. 30, 11379–11387. doi:10.1523/JNEUROSCI.2015-10.2010

Steriade, M., McCormick, D., Sejnowski, T., 1993. Thalamocortical oscillations in the sleeping and aroused brain. Science (80-.). 262, 679–685. doi:10.1126/science.8235588

Stevner, A.B.A., Vidaurre, D., Cabral, J., Rapuano, K., Nielsen, S.F. V., Tagliazucchi, E., Laufs, H., Vuust, P., Deco, G., Woolrich, M.W., Van Someren, E., Kringelbach, M.L., 2019. Discovery of key whole-brain transitions and dynamics during human wakefulness and non-REM sleep. Nat. Commun. 10, 1035. doi:10.1038/s41467-019-08934-3

Tagliazucchi, E., 2017. The signatures of conscious access and its phenomenology are consistent with large-scale brain communication at criticality. Conscious. Cogn. 55, 136–147. doi:10.1016/j.concog.2017.08.008

Tagliazucchi, E., Balenzuela, P., Fraiman, D., Chialvo, D., 2012. Criticality in large-scale brain FMRI dynamics unveiled by a novel point process analysis. Front. fractal Physiol. 3, 15. doi:10.3389/fphys.2012.00015

Tagliazucchi, E., Chialvo, D.R., Siniatchkin, M., Amico, E., Brichant, J.-F., Bonhomme, V., Noirhomme, Q., Laufs, H., Laureys, S., 2016a. Large-scale signatures of unconsciousness are consistent with a departure from critical dynamics. J. R. Soc. Interface 13, 20151027. doi:10.1098/rsif.2015.1027

Tagliazucchi, E., Crossley, N., Bullmore, E.T., Laufs, H., 2016b. Deep sleep divides the cortex into opposite modes of anatomical–functional coupling. Brain Struct. Funct. 221, 4221–

4234. doi:10.1007/s00429-015-1162-0

Tagliazucchi, E., von Wegner, F., Morzelewski, A., Brodbeck, V., Jahnke, K., Laufs, H., 2013. Breakdown of long-range temporal dependence in default mode and attention networks during deep sleep. Proc. Natl. Acad. Sci. 110, 15419–15424. doi:10.1073/pnas.1312848110

Tononi, G., Boly, M., Massimini, M., Koch, C., 2016. Integrated information theory: from consciousness to its physical substrate. Nat. Rev. Neurosci. 17, 450–461. doi:10.1038/nrn.2016.44

Turchi, J., Chang, C., Ye, F.Q., Russ, B.E., Yu, D.K., Cortes, C.R., Monosov, I.E., Duyn, J.H., Leopold, D.A., 2018. The Basal Forebrain Regulates Global Resting-State fMRI Fluctuations. Neuron 97, 940–952.e4. doi:10.1016/j.neuron.2018.01.032

Tzourio-Mazoyer, N., Landeau, B., Papathanassiou, D., Crivello, F., Etard, O., Delcroix, N., Mazoyer, B., Joliot, M., 2002. Automated anatomical labeling of activations in SPM using a macroscopic anatomical parcellation of the MNI MRI single-subject brain. Neuroimage 15, 273–289. doi:10.1006/nimg.2001.0978

Uhrig, L., Dehaene, S., Jarraya, B., 2014. A hierarchy of responses to auditory regularities in the macaque brain. J. Neurosci. 34, 1127–32. doi:10.1523/JNEUROSCI.3165-13.2014

Uhrig, L., Sitt, J.D., Jacob, A., Tasserie, J., Barttfeld, P., Dupont, M., Dehaene, S., Jarraya, B., 2018. Resting-state Dynamics as a Cortical Signature of Anesthesia in Monkeys. Anesthesiology 129, 942–958. doi:10.1097/ALN.0000000000002336

van den Heuvel, M.P., Sporns, O., 2011. Rich-club organization of the human connectome. J. Neurosci. 31, 15775–86. doi:10.1523/JNEUROSCI.3539-11.2011

van Vugt, B., Dagnino, B., Vartak, D., Safaai, H., Panzeri, S., Dehaene, S., Roelfsema, P.R., 2018. The threshold for conscious report: Signal loss and response bias in visual and frontal cortex. Science (80-.). 360, 537–542. doi:10.1126/science.aar7186

Vogt, B.A., Laureys, S., 2005. Posterior cingulate, precuneal and retrosplenial cortices: cytology and components of the neural network correlates of consciousness. Prog. Brain Res. 150, 205–17. doi:10.1016/S0079-6123(05)50015-3

Vyazovskiy, V. V., Olcese, U., Hanlon, E.C., Nir, Y., Cirelli, C., Tononi, G., 2011. Local sleep in awake rats. Nature 472, 443–447. doi:10.1038/nature10009

Wang, C., Ong, J.L., Patanaik, A., Zhou, J., Chee, M.W.L., 2016. Spontaneous eyelid closures link vigilance fluctuation with fMRI dynamic connectivity states. Proc. Natl. Acad. Sci. U. S. A. 113, 9653–8. doi:10.1073/pnas.1523980113

Wang, L., Uhrig, L., Jarraya, B., Dehaene, S., 2015. Representation of numerical and sequential patterns in macaque and human brains. Curr. Biol. 25, 1966–74. doi:10.1016/j.cub.2015.06.035

Wong, C.W., Olafsson, V., Tal, O., Liu, T.T., 2013. The amplitude of the resting-state fMRI global signal is related to EEG vigilance measures. Neuroimage 83, 983–990. doi:10.1016/j.neuroimage.2013.07.057

Yang, G.J., Murray, J.D., Glasser, M., Pearlson, G.D., Krystal, J.H., Schleifer, C., Repovs, G., Anticevic, A., 2014. Altered Global Brain Signal in Schizophrenia. Pnas 27, 5156–5169. doi:10.1093/cercor/bhw297

Zakszewski, E., Adluru, N., Tromp, D.P.M., Kalin, N., Alexander, A.L., 2014. A diffusion-tensor-based white matter atlas for rhesus macaques. PLoS One 9. doi:10.1371/journal.pone.0107398

Zamora-López, G., Zhou, C., Kurths, J., 2011. Exploring Brain Function from Anatomical Connectivity. Front. Neurosci. 5, 83. doi:10.3389/fnins.2011.00083

Zamora-López, G., Zhou, C., Kurths, J., 2010. Cortical hubs form a module for multisensory integration on top of the hierarchy of cortical networks. Front. Neuroinform. 4, 1. doi:10.3389/neuro.11.001.2010